Spatial variability of surface-water pCO_2 and gas exchange in the world's largest semi-enclosed estuarine system: St. Lawrence Estuary (Canada)

Ashley Dinauer[1] and Alfonso Mucci

GEOTOP and Department of Earth and Planetary Sciences, McGill University, 3450 University Street, Montreal, QC H3A 0E8, Canada

[1] Corresponding author (ashley.dinauer@mail.mcgill.ca)

Abstract

The incomplete spatial coverage of partial pressure of CO_2 (pCO_2) measurements across estuary types represents a significant knowledge gap in current regional- and global-scale estimates of estuarine CO_2 emissions. Given the limited research on CO_2 dynamics in large estuaries and bay systems, as well as the sources of error in the calculation of pCO_2 (carbonic acid dissociation constants, organic alkalinity contribution), estimates of estuarine CO_2 degassing may be overestimated. The Estuary and Gulf of St. Lawrence (EGSL) at the lower limit of the subarctic region in eastern Canada is the largest estuarine system in the world, and is characterized by an exceptional richness in environmental diversity. It is among the world's most intensively studied estuaries, yet there are no published data on its surface-water pCO_2 distribution. To fill this data gap, a comprehensive dataset was compiled from direct and indirect measurements of carbonate system parameters in the surface waters of the EGSL during the spring or summer of 2003–2016. The calculated surface-water pCO_2 ranged from 435–765 µatm in the shallow, partially mixed Upper Estuary, 139–578 µatm in the deep, stratified Lower Estuary, and 207–478 µatm along the Laurentian Channel in the Gulf. Overall, at the time of sampling, the St. Lawrence Estuary served as a very weak source of CO_2 to the atmosphere, with an area-averaged CO_2 degassing flux of 0.98 to 2.02 mmol C m^{-2} d^{-1} (0.36 to 0.74 mol C m^{-2} yr^{-1}). A preliminary analysis of factors controlling the spatial variability of surface-water pCO_2 revealed that respiration (Upper Estuary), photosynthesis (Lower Estuary), and temperature (Gulf) were dominant controls.

Keywords:
Coastal ocean, Estuaries, CO_2, Carbon cycle, Air-sea CO_2 exchange, St. Lawrence Estuary, Gulf of St. Lawrence, Laurentian Channel

1. Introduction

Although estuaries occupy a very small fraction (0.2 %) of the global ocean surface area, their CO_2 emissions are disproportionately large compared with CO_2 exchanges between the open ocean and the atmosphere (Bauer et al., 2013). With an estimated global efflux of 0.10–0.15 Pg C yr^{-1} (Chen et al., 2013; Laruelle et al., 2013), estuarine CO_2 degassing is thought to counterbalance CO_2 uptake on the continental shelves (Chen and Borges, 2009; Laruelle et al., 2010; Cai, 2011). Almost every estuary on Earth, for which data are available, is generally supersaturated with CO_2 with respect to the atmosphere (Cai and Wang, 1998; Frankignoulle et al., 1998; Borges, 2005; Borges et al., 2005; Borges et al., 2006; Chen and Borges, 2009; Laruelle et al., 2010; Cai, 2011; Chen et al., 2012; Bauer et al., 2013; Chen et al., 2013; Regnier et al., 2013), with CO_2 partial pressures (pCO_2) ranging from 400 to 10,000 µatm (in contrast, the atmospheric pCO_2 in coastal zones was approximately 360–385 µatm in year 2000) (Cai, 2011). Although estuaries are generally net sources of CO_2, there is considerable variability and uncertainty in estimates of their CO_2 emissions, reflecting the limited spatial and temporal coverage of pCO_2 measurements in estuaries as well as their heterogeneous nature (hydrological and geomorphological differences, differences in magnitude and stoichiometry of carbon and nutrient inputs) (Bauer et al., 2013; Regnier et al., 2013).

Estuaries are geochemical reaction vessels through which continentally weathered organic matter and inorganic nutrients must pass to enter the coastal ocean (Kaul and Froelich, 1984). Horizontal transport is controlled by a set of physical attributes (tides, wind, bathymetry, basin geography, river flow) that determine the estuarine filter function (Cloern, 2001). The longer the freshwater flushing (or turnover) time of the estuary, the more opportunity there is for water-column biological activity, benthic exchanges and particle-dissolved phase interactions to influence its biogeochemistry (Statham, 2012). DIC enrichments and pCO_2 supersaturations observed in estuaries can be mainly attributed to the *in situ* microbial degradation of internally and externally supplied organic carbon and the lateral transport of inorganic carbon from rivers, coastal wetlands and ground waters (Bauer et al., 2013).

In strongly tidal (macrotidal) systems, long water and particle residence times (on the order of weeks to months; Middelburg and Herman, 2007) allow for the extensive modification and degradation of particulate organic carbon during estuarine transport (Borges et al., 2006; Chen and Borges, 2009). In the absence of seasonal or permanent water stratification, the decoupling between production and degradation of organic matter at and below the surface, respectively, does not occur, resulting in less efficient export of dissolved inorganic carbon (Borges, 2005). Strongly tidal estuaries also tend to exhibit lower levels of photosynthetic activity (Monbet, 1992) and carry greater suspended particulate matter loads within their high-turbidity regions (Uncles et al., 2002; Middelburg and Herman, 2007) wherein suspended particles and organic-rich aggregates serve as "hot spots" of microbial recycling (Statham, 2012). Field measurements suggest that 10 % of the total CO_2 emissions from the inner estuary of macrotidal systems is sustained by the ventilation of riverine CO_2, whereas 90 % is due to local net heterotrophy (Borges et al., 2006) fueled by inputs of terrestrial and riverine-algae derived (planktonic) detritus and, in populated areas, sewage (Chen and Borges, 2009). In estuaries with long freshwater residence times, the riverine CO_2 will be fully ventilated to the atmosphere within the estuary, and the total CO_2 emissions can be attributed to net heterotrophy (Borges and Abril, 2011).

North American estuaries rank first in terms of global estuarine surface area (41 %) but account for the lowest numerically averaged CO_2 flux per unit area (12 %) among all continents (Chen et al., 2013). These estimates are subject to large uncertainties due to data paucity. A recent synthesis by Regnier et al. (2013) highlighted the meagre spatial coverage of estuarine pCO_2 measurements, particularly along the Canadian eastern seaboard. Ironically, the Estuary and Gulf of St. Lawrence (EGSL) in eastern Canada is the largest semi-enclosed estuarine system in the world, and is among the world's most intensively studied estuaries (El-Sabh and Silverberg, 1990), but was left unmentioned in recent global (Cai, 2011; Chen et al., 2012; Chen et al., 2013) and regional (Laruelle et al., 2015) data compilations. Furthermore, previous estuarine CO_2 studies have focused on small river-dominated estuaries, whereas there has been limited research on CO_2 dynamics in large estuaries and bays (Joesoef et al., 2015), i.e., marine-dominated systems, including the areas of mixing at sea (outer estuaries or river plumes) (Borges et al., 2005). A comparative study by Jiang et al. (2008) revealed large differences in CO_2 degassing between non-

105 riverine and river-dominated estuaries and, more recently, Koné et al. (2009), Maher
106 and Eyre (2012) and Cotovicz Jr. et al. (2015) reported small CO_2 uptake by strongly
107 stratified and/or marine-dominated systems. On the U.S. east coast, the ratio of non-
108 riverine (flushed by tidal action and receiving minimum freshwater inputs) to river-
109 dominated estuaries is nearly 1:1, demonstrating the geographic importance of
110 coastal estuaries/bays on the eastern seaboard of North America (Cai, 2011).
111
112 The large-scale (width often considerably greater than the internal Rossby
113 radius; Cyr et al., 2015), macrotidal (mean tidal range greater than 2–4 m; Monbet,
114 1992) St. Lawrence Estuary is an excellent analogue of marine-dominated systems.
115 Throughout its length, the full spectrum of oceanic variability can be found (Mertz and
116 Gratton, 1990). Moreover, the basin characteristics and water transport time scales of
117 the St. Lawrence Estuary provide an almost ideal natural laboratory for geochemical
118 studies. Its surface waters have a renewal time of several months while its bottom
119 waters take several years to replenish, allowing for a comparison of spatial-temporal
120 variations in physical and chemical properties (El-Sabh and Silverberg, 1990). Given its
121 bimodal bathymetry, the St. Lawrence Estuary also permits the investigation of
122 biogeochemical processes in two types of estuary: (1) the shallow, partially mixed
123 Upper Estuary where physical mixing and abiotic processes dominate, and (2) the
124 deep, stratified Lower Estuary where biological cycling and oceanic processes prevail
125 (Yeats, 1990). As yet, no systematic study of the CO_2 dynamics in the St. Lawrence has
126 been published and, hence, the present study provides the first comprehensive
127 description of its mixed-layer carbonate chemistry, including (1) a multi-year
128 compilation of springtime and summertime pCO_2 calculated from direct
129 measurements of pH and alkalinity; (2) an area-averaged estimate of the air-sea CO_2
130 gas flux; and (3) an analysis of the relative importance of thermodynamic (temperature)
131 and biological (photosynthesis, respiration) processes in controlling the spatial
132 variability of surface-water pCO_2.
133
134 **2. Materials and methods**
135
136 **2.1. Study area—St. Lawrence Estuary and Gulf**
137

138 The greater St. Lawrence system (Fig. 1) connects the chain of Great Lakes, the
139 second largest terrestrial freshwater reservoir in the world, to the Atlantic Ocean (Yang
140 et al., 1996). With a drainage basin of approximately 1.32 million km^2, the St. Lawrence
141 River channels the second largest freshwater discharge (11,900 $m^3 s^{-1}$) on the North
142 American continent, second only to that of the Mississippi (El-Sabh and Silverberg,
143 1990). The catchment area geology is dominated by silicate rocks of the Precambrian
144 Shield and carbonates of the Paleozoic lowlands, whose components influence the
145 downstream evolution of river chemistry (Yang et al., 1996). The erosion of the
146 carbonate rocks of the drainage basin is practically constant, as the quantity of
147 bicarbonate ions carried by the river varies little from season to season (Pelletier and
148 Lebel, 1979). On a yearly basis, between 15–20 % of the outflow of dissolved inorganic
149 carbon from the St. Lawrence River into its estuary originates from the system's
150 tributaries (e.g., Ottawa River, Mascouche River) while 80–85 % is from the Great Lakes
151 (Hélie et al., 2002). The St. Lawrence Estuary (SLE) begins at the landward limit of the
152 salt water intrusion near Île d'Orléans (~5 km downstream of Québec City) and
153 stretches 400 km seaward to Pointe-des-Monts where it widens into the Gulf of St.
154 Lawrence (GSL) (El-Sabh and Silverberg, 1990), a semi-enclosed sea with an area of
155 approximately 240,000 km^2 (Dufour and Ouellet, 2007) connected to the Atlantic
156 Ocean through Cabot Strait and the Strait of Belle Isle (Coote and Yeats, 1979).
157
158 Traditionally, the SLE is divided into two segments based on its bathymetry and
159 hydrographical features (Ingram and El-Sabh, 1990). The Upper St. Lawrence Estuary
160 (USLE), from Île d'Orléans, where the estuarine circulation begins, to Tadoussac, near
161 the mouth of the Saguenay Fjord, covers an area of 3,470 km^2. It is relatively narrow (2
162 to 24 km wide) and mostly shallow (depths less than 30 m; d'Anglejan, 1990), and
163 features an uneven, fairly complex bottom topography characterized by several
164 disconnected channels and troughs separated by ridges and islands (El-Sabh and
165 Murty, 1990). Topographically modified flows give rise to very large tidal ranges and
166 currents (up to 10 m and 3 m s^{-1}, respectively; Mertz and Gratton, 1990). In this tidally
167 energetic region, wind mixing is one to two orders of magnitude smaller than tidal
168 mixing (Painchaud et al., 1995). Owing to the resuspension of bottom sediments (tide,
169 wind or wave generated) and the net non-tidal estuarine circulation (d'Anglejan and
170 Smith, 1973), a well-developed turbidity maximum stretches between Île d'Orléans
171 and Île-aux-Coudres (Painchaud and Therriault, 1989) where suspended particulate

matter concentrations vary from 10 to more than 200 mg l^{-1} (Silverberg and Sundby, 1979). The sources of particulate organic matter (POM) in the estuary are still debated (Gearing and Pocklington, 1990). Carbon isotope studies indicate that less than half of the POM is derived from terrestrial sources (Pocklington and Leonard, 1979) and is quite refractory to biodegradation (Lucotte et al., 1991), whereas the major contributor to POM is believed to be "fresh" organic matter, i.e., living or recently living material, of river-borne origin (Tan and Strain, 1983; Hélie and Hillaire-Marcel, 2006). During the spring freshet in April–May, when freshwater discharge delivers 40 % of the annual solid inputs to the estuary, the input of terrigenous POM is equivalent to the average POM kept in suspension in the turbidity maximum (Lucotte, 1989).

The Lower St. Lawrence Estuary (LSLE) is fairly unique in that its character is more oceanic than most estuaries due to its grand size in all three dimensions and unimpeded connection with Labrador and Slope waters from the Atlantic Ocean (El-Sabh and Silverberg, 1990). Relative to the USLE, the LSLE is much larger (9,350 km^2; d'Anglejan, 1990), wider (30 to 50 km) and deeper (~300 m), and displays a smoother, less variable bottom topography. Tidal currents are weaker (on the order of 30 cm s^{-1} or less; Mertz and Gratton, 1990) and, under these less turbulent conditions, the Lower Estuary is the major sink of continental inputs to the St. Lawrence system. Most (~75 %) of the terrigenous POM carried by the St. Lawrence River is deposited on the LSLE floor (Lucotte et al., 1991). The dominant bathymetric feature of the LSLE is the Laurentian Channel (or Trough), a deep, central, U-shaped glaciated valley that extends 1,240 km from the eastern Canadian continental shelf break through the GSL and into the LSLE (d'Anglejan, 1990). The termination (head) of the Laurentian Channel at an abrupt and shallow sill near Tadoussac marks the region of transition between the Upper and Lower Estuary and is an area of complex tidal phenomena (Gratton et al., 1988). Due to rapid shoaling, tidal movements (e.g., internal tides and strong flows over the steep sill) locally generate significant mixing of surface freshwater with cold, nutrient-rich waters from the intermediate and deep layers of the Gulf, resulting in a fertile surface layer that flows continuously seaward (Coote and Yeats, 1979; Saucier and Chassé, 2000) and sustains important feeding habitats for several large marine mammals (Dufour and Ouellet, 2007). The Lower Estuary's seaward outflow, together with the Gaspé Current, a rapidly moving coastal jet, are a major input of nutrients and zooplankton to the near-surface waters of the GSL (Coote and Yeats, 1979; Plourde

and Runge, 1993). Mesoscale features such as coastal jets, internal Kelvin waves, baroclinic eddies and unstable waves are all possible due to strong Coriolis effects (Ingram and El-Sabh, 1990).

The Lower St. Lawrence Estuary is one of the most laterally stratified estuaries in the world (Larouche et al., 1987), and is also strongly vertically stratified. During summertime, the SLE can be described as a three-layer system on the basis of its thermal stratification (Gratton et al., 1988). Each spring, a new surface layer flow is initiated by the freshwater runoff from the St. Lawrence River, Saguenay Fjord and rivers on the north shore of the estuary (Dufour and Ouellet, 2007; see Fig. 1). Discharge from the St. Lawrence River (mean annual discharge of 10,000 m^3 s^{-1}, peaking at 15,000 m^3 s^{-1} during the spring freshet; Painchaud and Therriault, 1989) provides about 80 % of the total freshwater input to the estuary (Ingram and El-Sabh, 1990), whereas the combined runoff from the Saguenay and Manicouagan Rivers accounts for most of the remainder (Tee, 1990). The warm and relatively fresh surface layer (0 to 30 m) overlies the cold intermediate layer or CIL (30–150 m deep; S_P = 32.0 to 32.6) that is formed by advection of the Gulf's wintertime surface mixed layer (Galbraith, 2006). Below the CIL, a warmer (2 to 6 °C) and saltier (S_P = 33 to 35) bottom layer (>150 m deep), originating from the mixing of western-central Atlantic and Labrador shelf waters that intrude at depth primarily through Cabot Strait, flows sluggishly landward (~0.5 cm s^{-1}; Bugden, 1988) toward the head region of the Laurentian Channel (Saucier et al., 2003; Gilbert et al., 2005).

2.2. Water-column sampling and analytical procedures

Water samples were collected aboard the RV *Coriolis II* during ten research cruises within the St. Lawrence Estuary and Gulf in the ice-free spring or summer season between 2003 and 2016. Water sampling was conducted mainly along the central axis of the St. Lawrence Estuary and the Laurentian Channel. The sampling locations are shown in Fig. 2. Samples were taken from discrete depths throughout the water column, typically at 3 m, 20 m, 50 m, 70 m, 100 m and at 50m intervals to the bottom (or within 10 m of the bottom). A comprehensive dataset was compiled from field or laboratory measurements of the following physical–chemical properties: temperature (T), practical salinity (S_P), pH_{NBS} and/or pH_T, total alkalinity (TAlk), dissolved inorganic

carbon (DIC), soluble reactive phosphate (SRP), and dissolved silicate (DSi), nitrate (NO_3) and oxygen (DO).

T and S_P were determined *in situ* using the conductivity-temperature-depth (CTD) probe (SeaBird SBE 911) mounted on the sampling rosette. The temperature probe was calibrated by the manufacturer, whereas the conductivity sensor was calibrated by the manufacturer and recalibrated using discrete salinity samples collected throughout the water column and analyzed on a Guildline Autosal 8400 salinometer calibrated with IAPSO standard seawater. Water samples destined for pH and TAlk measurements were transferred directly from the 12L Niskin bottles mounted on the CTD-rosette system to, respectively, 125mL plastic bottles without headspace and 250mL glass bottles as soon as the rosette was secured onboard. In the latter case, a few crystals of $HgCl_2$ were added before the bottle was sealed with a ground-glass stopper and Apiezon® Type-M high-vacuum grease.

pH was determined onboard at 25 °C, potentiometrically on the NBS/NIST scale (infinite dilution convention, pH_{NBS}) for low salinity waters ($S_P < 5$) and potentiometrically and/or colorimetrically on the total hydrogen ion concentration scale (constant ionic medium convention, pH_T) for higher salinity waters. Potentiometric pH measurements were carried out using a Radiometer Analytical® GK2401C combination glass electrode connected to a Radiometer Analytical® PHM84 pH/millivolt-meter. Prior to each measurement, the electrode was calibrated against three NIST-traceable buffer solutions: pH-4.00, pH-7.00 and pH-10.00 at 25°C. The electrode response to these buffers was then least-squares fitted to obtain the Nernstian slope. For $S_P > 5$, pH measurements were converted to the pH_T scale using TRIS buffer solutions prepared at S_P = 5, 15, 25, or 35 for which the pH_T was assigned at 25°C (Millero, 1986). Colorimetric pH measurements were carried out using a Hewlett-Packard UV-Visible diode array spectrophotometer (HP-8453A) and a 5cm quartz cell after thermal equilibration of the plastic sampling bottles in a constant temperature bath at 25.0 ± 0.1°C. Phenol red (Robert-Baldo et al., 1985) and *m*-cresol purple (Clayton and Byrne, 1993) were used as color indicators. The pH_T of the water samples and buffer solutions were calculated according to the equation of Byrne (1987). The reproducibility of the pH measurements was typically better than ± 0.003.

TAlk was measured at McGill University using an automated Radiometer (TitraLab865®) potentiometric titrator and a Red Rod® combination pH electrode (pHC2001). The dilute HCl titrant was calibrated prior, during, and after each titration session using certified reference materials provided by Andrew Dickson (Scripps Institute of Oceanography). Raw titration data were processed with a proprietary algorithm specifically designed for shallow end-point detection. The reproducibility of the method was better than 0.5 %.

Direct DIC measurements were carried out during an additional cruise in 2014 using a Scitech Apollo DIC analyzer. After being thermostated at 25 °C, 1–1.5 mL of the sample was injected into the instrument's reactor where it was acidified with 10 % H_3PO_4 and the evolved CO_2 carried by a stream of pure nitrogen to a LICOR infrared analyzer. A calibration curve was constructed using gravimetrically-prepared Na_2CO_3 solutions, and the accuracy of the measurements was verified using certified reference material solutions provided by Andrew Dickson (Scripps Institute of Oceanography). The reproducibility of the measurements was typically on the order of 0.2 %. Results of the direct DIC measurements were used to assess the contribution of organic alkalinity to the total alkalinity in the Upper Estuary, as discussed in Section 2.3.2.

DO concentrations were determined by Winkler titration (Grasshoff et al., 1999) on distinct water samples recovered directly from the Niskin bottles. The relative standard deviation, based on replicate analyses of samples recovered from the same Niskin bottle, was better than 1 %. These measurements further served to calibrate the SBE-43 oxygen probe mounted on the rosette. For the determination of nutrient concentrations, aliquots of the water samples taken from the Niskin bottles were syringe filtered through a 0.45µm Millipore polycarbonate (MA) filter. DSi was measured onboard on the same day of sampling using the method described in Grasshoff et al. (1999). Water samples destined for NO_3 and SRP measurements were transferred, respectively, into acid-washed 15ml polyethylene and borosilicate tubes, quickly frozen and stored at –20 °C. Their concentrations were determined using standard colorimetric methods adapted from Grasshoff et al. (1999) with a SEAL Autoanalyzer III at the Institut des Sciences de la Mer de Rimouski. The analytical detection limit was 0.04 µM for NO_3, 0.05 µM for SRP and 0.1 µM for DSi. Based on

replicate analyses of the standards, the reproducibility of these measurements was typically 1 %.

The *in situ* pressure and density of the samples were calculated from the Thermodynamic Equation of Seawater – 2010 (TEOS-10) using the Gibbs Seawater (GSW) Oceanographic Toolbox (MATLAB-version 3.05; McDougall and Barker, 2011). All field measurements reported in μmol L^{-1} were converted to μmol kg^{-1} using the *in situ* density data.

2.3. Calculation of aqueous pCO_2

2.3.1. pCO_2 in mixed-layer waters

Aqueous pCO_2 (pCO_2(water)) is defined as the partial pressure of carbon dioxide in wet (100 % water-saturated) air that is in equilibrium with the water sample. Because direct pCO_2 measurements were not available from the RV *Coriolis II* cruises, pCO_2(water) (μatm) and DIC (μmol kg^{-1}) were calculated from the measured pH (total or NBS scale) and TAlk (μmol kg^{-1}), at *in situ* temperature (°C), salinity (S_P) and pressure (dbar), using the program CO2SYS (MATLAB-version 1.1; van Heuven et al., 2011) and the carbonic acid dissociation constants (K_1, K_2) of Cai and Wang (1998) for estuarine waters. Wherever data were available, the contributions to TAlk from phosphate and silicate were included in the calculations. Although the K_1 and K_2 formulations from Lueker et al. (2000) are recommended for best practices by Dickson et al. (2007), they are not suitable for the low-salinity conditions found in estuaries (S_P < 19) (Orr et al., 2015). The revised equations for K_1 and K_2 from Cai and Wang (1998) are applicable over a larger range of salinities (0 to 40) and, thus, were used to examine the carbonate system in the estuarine waters of our study area.

This study focuses on the CO_2 dynamics in near-surface waters. To obtain individual data points of surface-water pCO_2 at each sampling location, the pCO_2 data in the surface mixed layer (SML) were averaged. The SML is the site of active air-sea interaction where heat and gases are exchanged directly with the atmosphere and within which physical (temperature, salinity, density) and chemical (dissolved gases) properties are vertically homogeneous due to turbulent mixing (Sprintall and Tomczak,

1992). The lower limit to air-sea interaction, i.e., the mixed layer depth (MLD), is demarcated by a pycnocline, a sharp density gradient that generally coincides with both a temperature (thermocline) and salinity (halocline) gradient. Here, we determine the thickness of the SML using a density-based criterion which defines the MLD as the depth at which a threshold difference of 0.03 kg m^{-3} from the sea surface occurs (de Boyer Montégut et al., 2004). In the following sections, surface-water pCO_2 will be taken to mean the SML-averaged pCO_2.

2.3.2. Sources of error in pCO_2 calculation

In this study, pH/TAlk was used as the input combination to study the consistency between calculations of pCO_2 using different sets of carbonic acid dissociation constants. The importance of using appropriate formulations of K_1 and K_2 in estuarine waters is shown by the discrepancies in the calculated pCO_2 values (pCO_2 @ 15 °C) at low salinities (Fig. 3). The percent difference between values calculated using the dissociation constants of Cai and Wang (1998) and those calculated using the best-practices constants of Lueker et al. (2000) was on average 3.07 %. At $S_P < 19$, differences between the calculated pCO_2 values were as large as 18.0 % (average difference of 6.88 %), whereas, at $S_P > 19$, the calculated values were in better agreement (only ~1.48 % difference). The K_1 and K_2 formulations of Millero (2010), the most recent set of constants proposed for estuarine waters (S_P = 1 to 50), yielded pCO_2 values that differed substantially from those derived using the constants of Cai and Wang (1998) at $S_P < 19$, with the largest divergence reaching 34.4 % (average difference of 13.6 %). At $S_P = 0$, the pCO_2 values calculated using the constants of Cai and Wang (1998) compared very well with those given by the Millero (1979) constants for freshwater (difference of only ~0.08 %), whereas the pCO_2 values calculated using the constants of Millero (2010) showed very poor agreement with the freshwater results (differing by ~34.3 %). These discrepancies highlight the need for new or revised measurements of the carbonic acid dissociation constants under estuarine conditions (in brackish waters) especially at $S_P < 5$. Studies which use the best-practices formulations of K_1 and K_2 to calculate estuarine pCO_2 may underestimate CO_2 emissions at low salinities, whereas those that implement the Millero (2010) formulations may produce overestimates.

Another potential source of error in the calculation of pCO_2 (pH/TAlk) in low-salinity estuarine waters is the contribution of dissolved organic compounds to the total alkalinity. The contributions of borate, phosphate and silicate species are taken into consideration in CO2SYS, whereas the magnitude of organic alkalinity (Org-Alk, or excess alkalinity) is usually assumed to be small or negligible, and is simply ignored when using TAlk to calculate pCO_2 in open ocean waters. In riverine and coastal waters, however, the contribution of organic species to the TAlk can be significant (Yang et al., 2015). Rivers draining organic-rich soils and non-carbonate rocks have low DIC concentrations (a few hundred μmol L^{-1}) that are often exceeded by dissolved organic carbon (DOC) concentrations (Abril et al., 2015). As discussed by Hunt et al. (2011), a significant contribution of Org-Alk (the organic acid anions in DOC) leads to an overestimation of calculated pCO_2 using any algorithm that accounts only for the contributions of inorganic species to TAlk. A comparison of the calculated TAlk (DIC/pH) and the measured TAlk from the 2014 cruise reveals that Org-Alk is on the order of –20 μmol kg^{-1} for the St. Lawrence River end-member, whereas it is as high as –120 μmol kg^{-1} for the Saguenay River end-member (A. Mucci, pers. comm.). Given that TAlk exceeds ~1000 μmol kg^{-1} throughout our study area and the Saguenay River contribution to the surface waters of the SLE is limited (at most ~6 % at the head of the Lower Estuary; Mucci et al., in revision), consideration of the Org-Alk in the calculation of pCO_2 (pH/TAlk) yielded values that were at most 1.9 % different from those uncorrected for Org-Alk. Bearing in mind the uncertainties in the K_1 and K_2 formulations as well as the analytical uncertainties, the influence of Org-Alk on the calculated pCO_2 (pH/TAlk) did not represent a significant source of error.

2.4. Temperature normalization of pCO_2

The effect of temperature on aqueous pCO_2 is primarily the manifestation of changes in the solubility of CO_2 gas in water (Takahashi et al., 1993). The temperature dependence of pCO_2 in seawater, i.e., $\partial \ln(pCO_2) / \partial T = 0.0423\ °C^{-1}$, was determined experimentally by Takahashi et al. (1993) on a single North Atlantic surface water sample with $S_P = 35.380$ under isochemical conditions. As this oft-used approximation for thermally induced changes in pCO_2 was derived from direct measurements in open ocean waters, we use a different approach to remove the temperature effect on the estuarine pCO_2 in our study area. The *in situ* pCO_2 were normalized to the average

surface-water temperature ($pCO_2(\overline{SST})$, $\overline{SST}$ = 7.82 °C), using the temperature normalization method of Jiang et al. (2008) in which pCO_2 values are re-calculated from the TAlk and DIC data at a common temperature. The results yielded a temperature coefficient of ∂ ln(pCO_2) / ∂T = 0.0402 °C^{-1} (R^2= 0.99), in excellent agreement with that of Takahashi et al. (1993). The pCO_2 changes due to temperature deviations from $\overline{SST}$ (ΔpCO_2(temp)) were calculated as:

$$\Delta pCO_2(temp) = pCO_2(obs) - pCO_2(\overline{SST}) \quad (1)$$

where pCO_2(obs) is the *in situ* pCO_2 and $pCO_2(\overline{SST})$ is the temperature-normalized pCO_2. Since changes in pCO_2 at a common temperature primarily reflect changes in DIC, the spatial variations in $pCO_2(\overline{SST})$ can be attributed to the combined influences of non-thermal processes that affect DIC (water mass mixing, biological activity). Theoretically, $pCO_2(\overline{SST})$ can be further partitioned into the pCO_2 change due to biology and that due to mixing through an analysis of the water mass structure, e.g., an optimum multiparameter (OMP) water mass analysis. Results from its application will be presented in a subsequent study.

2.5. Air-sea CO_2 flux estimation

Air-sea CO_2 gas exchange (F, mmol C m^{-2} d^{-1}) at each sampling location was estimated as follows:

$$F = k \cdot K_0 \cdot \left(pCO_2(water) - pCO_2(air)\right) \quad (2)$$

where k (cm h^{-1}) is the gas transfer velocity of CO_2, K_0 (mol kg^{-1} atm^{-1}) is the solubility coefficient of CO_2 at *in situ* surface-water temperature and salinity (Weiss, 1974), and pCO_2(water) and pCO_2(air) (µatm) are the partial pressures of CO_2 in the water and the air, respectively. The difference between pCO_2(water) and pCO_2(air) (ΔpCO_2) determines the direction of gas exchange across the air-sea interface. Positive values of F indicate CO_2 release by the surface water, whereas negative values indicate CO_2 uptake. Conversion factors were applied to express the final F with the aforementioned units.

Atmospheric pCO_2 (pCO_2(air)) was calculated using the monthly averages of the measured mole fraction of CO_2 in dry air (xCO_2, at the greenhouse gas observational station in Fraserdale, Ontario) obtained from the Climate Research Division at Environment and Climate Change Canada. The mean pCO_2(air) in the sampling month was computed using the relationship (Takahashi et al., 2002):

$$pCO_2(air) = xCO_2 \cdot (P_b - P_w) \quad (3)$$

where xCO_2 is in ppm, P_b (atm) is the atmospheric (or barometric) pressure at the sea surface, and P_w (atm) is the equilibrium (or saturation) water vapor pressure at *in situ* surface-water temperature and salinity (Weiss and Price, 1980). One-month averaged barometric pressures were calculated using the hourly station pressure data from Environment Canada at the following weather observing stations: Québec/Jean Lesage International Airport (Upper Estuary), Mont-Joli Airport (Lower Estuary), and Gaspé Airport (Gulf of St. Lawrence). The P_b at station elevation was converted to mean sea level pressure using the formula of Tim Brice and Todd Hall (NOAA's National Weather Service, http://www.weather.gov/epz/wxcalc_stationpressure).

The formulation of the gas transfer velocity, k, is the largest source of error in the computation of air-sea CO_2 fluxes (Borges et al., 2004a,b). Properly constraining values of k in estuaries is problematic (Raymond and Cole, 2001) due to their hydrodynamic and geomorphologic complexity (Abril et al., 2000). Gas transfer is thought to be regulated by turbulence at the air-water interface (Wanninkhof, 1992). Wind stress plays a key role in the generation of turbulence at the ocean surface through the transfer of momentum to waves and currents (Ho et al., 2011), whereas, in estuarine environments and especially macrotidal estuaries, surface turbulence can be created by interactions of wind forcing, tidal currents and boundary friction (Zappa et al., 2003, Borges et al., 2004a,b; Zappa et al., 2007) and, in turbid estuaries, attenuated by suspended material (Abril et al., 2009). The turbulence generated from bottom stress varies with water depth and tidal velocity (Raymond et al., 2000), and is important only in shallower estuaries with high current velocities (Cerco, 1989). Raymond and Cole (2001) have shown that wind stress controls turbulence at the air-water interface for all systems with depths greater than 10 meters (at depths < 10 m, either wind or bottom stress may dominate).

Several different predictive relationships between wind speed and gas transfer velocity have been proposed based on laboratory and field studies. Here, we estimate the latter from short-term (or steady) wind speed measurements using the equations of Wanninkhof (1992) revised by Wanninkhof (2014) and Raymond and Cole (2001):

k from Wanninkhof (2014), denoted as $k_{W\text{-}14}$:

$$k_{W-14} = 0.251\, u^2 (Sc\ /\ 660)^{-0.5} \quad (4)$$

k from Raymond and Cole (2001), denoted as $k_{R\&C\text{-}01}$:

$$k_{R\&C-01} = 1.91\, e^{0.35u} (Sc\ /\ 660)^{-0.5} \quad (5)$$

where u is the wind speed (m s^{-1}) and Sc is the Schmidt number (Sc = μ/D, where μ is the kinematic viscosity of the water and D is the diffusion coefficient) for CO_2 gas in solution. The Schmidt number for CO_2 in seawater at 20 °C is 660 and was adjusted to Sc=600 for freshwater. Hourly wind speed data were obtained from Environment Canada at the aforementioned weather observing stations, and averaged over the sampling month to obtain short-term wind speeds. The correction to a common Schmidt number was performed using the equations of Wanninkhof (1992) for the temperature dependence of Sc for CO_2 gas in seawater (S_P=35) and freshwater, respectively, and assuming that k is proportional to $Sc^{-0.5}$.

Because of increased turbulence, one would expect k values calculated from estuarine parameterizations to be higher than those predicted from oceanic parameterizations at equivalent wind speeds (Abril et al., 2000). Within the confines of the SLE, estimates of k using the Wanninkhof (2014) relationship ranged from 1.6 to 4.5 cm h^{-1} whereas those calculated from Raymond and Cole (2001) were between 3.8 and 8.1 cm h^{-1}. Hence, we take the air-sea CO_2 flux values calculated with $k_{W\text{-}14}$ to be the theoretical lower limit of gas exchange ($F_{W\text{-}14}$), whereas those computed from $k_{R\&C\text{-}01}$ represent the upper limit of gas exchange ($F_{R\&C\text{-}01}$).

In order to estimate the area-averaged CO_2 flux in the SLE, the estuary proper was divided into five segments, with each section containing at least one sampling location. Given that the Lower Estuary occupies ~75 % of the total estuarine surface

area, and encompasses a fairly wide range of pCO_2 values (standard deviation of 119 µatm), the SLE was divided into longitudinal sections (Fig. 2) rather than segmented by salinity. The fluxes in each segment were normalized to the sectional surface area and then summed to obtain a spatially integrated air-sea CO_2 flux ($F_{area\text{-}avg}$) for the whole estuary, as follows (Jiang et al., 2008):

$$F_{area-avg} = \frac{\sum F_i \cdot S_i}{\sum S_i} \quad (6)$$

where F_i is the average of all the fluxes within segment i, and S_i is the surface area of segment i. Sectional surface areas were tabulated in MATLAB using the land mask of eastern Canada obtained from Fisheries and Oceans Canada. An area-averaged CO_2 flux was obtained for both the upper and lower limits of gas exchange in the SLE. These two final estimates are assumed to bracket the real areal CO_2 flux.

2.6. Conceptual framework for the analysis of variations in biogenic gas concentrations

A comparison of the distribution of biologically reactive dissolved gases, i.e., CO_2 and O_2, can provide useful information about the physical (thermal) and biological processes controlling their concentrations (Richey et al., 1988). Temperature-related gas solubility effects occur in the same direction for CO_2 and O_2, whereas biological production and respiration affect CO_2 and O_2 in opposite directions. Following the approach of Carrillo et al. (2004), the saturation states (or % saturation) of pCO_2 and DO, with respect to the atmosphere, were compared in order to determine the relative importance of temperature effects (heating or cooling) and biological activity (photosynthesis or respiration) in the surface waters at each sampling location. The pCO_2 percent saturation (pCO_2(% sat)) was calculated as follows:

$$pCO_2(\%\, sat) = \left(pCO_2(water) \,/\, pCO_2(air)\right) \cdot 100 \quad (7)$$

The DO percent saturation (DO(% sat)) was calculated as:

$$DO(\%\, sat) = (DO/DO^*) \cdot 100 \quad (8)$$

where DO^* is the equilibrium DO concentration (μmol kg^{-1}) at *in situ* surface-water temperature and salinity (Benson and Krause, 1984). The relationship between DO(% sat) and pCO_2(% sat) is roughly analogous to that of the apparent oxygen utilization (AOU) and excess DIC (eDIC) (Abril et al., 2000). The former is defined as the difference between DO^* and DO, whereas the latter is defined as the difference between the observed DIC and a theoretical DIC at atmospheric equilibrium.

According to the method of Carrillo et al. (2004), data points fall into one of four quadrants on a graph of DO(% sat) versus pCO_2(% sat), with the origin at 100 % saturation for both gases. Quadrant I (upper left; supersaturated DO, undersaturated pCO_2) suggests net photosynthesis, Quadrant II (upper right; supersaturated DO and pCO_2) indicates the effects of heating, Quadrant III (lower right; undersaturated DO, supersaturated pCO_2) implies net respiration, and Quadrant IV (lower left; undersaturated DO and pCO_2) represents the effects of cooling. Although general patterns become apparent, we urge caution in the interpretation of these results as significant limitations apply. Surface-water CO_2 and O_2 may be acted upon by other forcings such as air-sea gas exchange. The net transfer of CO_2 and O_2 gases occurs across the air-sea interface whenever their partial pressures in the SML differ from those in the atmosphere. Because of their differential gas exchange rates (i.e., O_2 exchanges ~19 times faster than CO_2; Peng et al., 1987), CO_2 and O_2 dynamics may be decoupled in surface waters, causing an asymmetry in the observed CO_2:O_2 relationship (Carrillo et al., 2004).

3. Results and discussion

3.1. Spatial variability of surface-water pCO_2

Data were compiled from all ten cruises to describe the inorganic carbon chemistry in the mixed-layer waters of the St. Lawrence River, Upper Estuary, Lower Estuary and Gulf (Table 1). Large spatial variations in surface-water pCO_2 were observed within the EGSL system, with values ranging from 139 to 765 μatm (452 ± 134 μatm) during the spring/summer sampling periods. Overall, the pCO_2 were higher in the USLE (571 ± 72 μatm) than in the LSLE (394 ± 119 μatm) and GSL (352 ± 80 μatm), whereas the atmospheric pCO_2 showed less variability, ranging from 372 to 405 μatm,

during the sampling years. As shown in Fig. 4, the USLE was always a CO_2 source (i.e., surface-water pCO_2 were above atmospheric level) while the LSLE and GSL were generally either a CO_2 sink or nearly neutral (i.e., surface-water pCO_2 were below or close to atmospheric level).

Within the confines of the SLE, the surface-water pCO_2 generally decreased with increasing distance from the head of the estuary (Île d'Orléans) and along the salinity gradient (Fig. 4 and 5). The highest values of pCO_2 were observed near the landward limit of the salt water intrusion in the SLE's upper reaches, in the vicinity of the Cap Tourmente intertidal flats and marshes. This area (3×10^6 m^2) is located along the core of the estuary's maximum turbidity zone (MTZ) (Lucotte and d'Anglejan, 1986). The lowest surface-water pCO_2 were found downstream of the MTZ in the lower reaches of the SLE near Pointe-des-Monts, where the channel widens into the gulf. Due to favorable environmental conditions (nutrients, light, stratification), phytoplankton blooms typically occur in late spring or early summer in the LSLE (Zakardjian et al., 2000), with maximal biological production occurring in its downstream portion due to the mixing of cold, nutrient-rich waters, upwelled at the head of the Laurentian Channel, with warmer freshwaters flowing in from the north shore rivers (Savenkoff et al., 1994). Seaward from the estuary-gulf boundary, the pCO_2 gradually increased from 207 to 478 µatm, coinciding with rising surface-water temperatures (T = 3.9 to 13.7 °C).

The spatial variability of surface-water pCO_2 due to temperature variations was removed by normalizing the pCO_2 data to a common temperature (T = 7.82 °C). From a comparison of the *in situ* and corresponding temperature-normalized pCO_2, spatial variations in surface-water temperature lowered or raised the pCO_2 by –122 to 181 µatm within the EGSL system. The maximum (minimum) values of $\Delta pCO_2(temp)$, expressed as a percent change, were 38 % (–14 %) in the USLE, 24 % (–20 %) in the LSLE, and 29 % (–17 %) in the GSL. Temperature normalization, however, removed only a small part of the overall spatial variability of surface-water pCO_2 (Fig. 6). Given that the spread of the $pCO_2(\overline{SST})$ data remained large (153–668 µatm; 447 ± 133 µatm), most of the spatial variability in surface-water pCO_2 can be explained by non-thermal physical and biological processes that affect DIC concentrations in the mixed layer.

3.2. Air-sea CO_2 flux and spatial integration

Large spatial variations in the air-sea CO_2 flux were observed within the EGSL system during the spring/summer sampling months, with fluxes ranging from –21.9 to 28.4 mmol m^{-2} d^{-1} (Fig. 7). Values of F were always positive in the USLE (2.0 to 28.4 mmol m^{-2} d^{-1}) and either negative or positive in the LSLE (–21.9 to 15.1 mmol m^{-2} d^{-1}) and GSL (–8.4 to 3.6 mmol m^{-2} d^{-1}). As expected, $F_{R\&C\text{-}01}$ (estuarine parameterization of k) were larger than $F_{W\text{-}14}$ (oceanic parameterization of k) due to the inherently greater surface turbulence in estuarine systems. The average difference between CO_2 fluxes calculated using the two formulations of the gas transfer velocity (equations 4 and 5) was 71.7 %. Details of the k and F values given by each parameterization of k are shown in Table 2. Irrespective of the parameterization, the calculated CO_2 fluxes were more positive in the USLE (9.2 ± 5.3 mmol m^{-2} d^{-1}) than in the LSLE (0.8 ± 7.2 mmol m^{-2} d^{-1}) and GSL (–1.2 ± 3.0 mmol m^{-2} d^{-1}).

The SLE was divided into five segments to obtain an area-averaged CO_2 flux for the whole estuary. The data used to calculate the $F_{area\text{-}avg}$ are listed in Table 3. Overall, the SLE served as a weak source of CO_2 to the atmosphere at the time of sampling, with an area-averaged degassing flux of 0.98 to 2.02 mmol C m^{-2} d^{-1} (0.36 to 0.74 mol C m^{-2} yr^{-1}) during the late spring and early summer. This efflux compares favorably with that of the Delaware Estuary (2.4 ± 4.8 mol C m^{-2} yr^{-1}; Joesoef et al., 2015), another large estuarine system with a long water residence time, but is significantly lower than estimates in the marine-dominated Sapelo and Doboy Sound estuaries (10.5 to 10.7 mol C m^{-2} yr^{-1}; Jiang et al., 2008). From a compilation of 165 estuaries worldwide, almost all systems, with the exception of those in the Arctic (–1.1 mol C m^{-2} yr^{-1}), serve as sources of CO_2 to the atmosphere (Chen et al., 2013). Chen et al. (2013) concluded that the world's upper estuaries (S_P < 2) are strong sources (39.0 ± 55.7 mol C m^{-2} yr^{-1}), mid estuaries (2 < S_P < 25) are moderate sources (17.5 ± 34.2 mol C m^{-2} yr^{-1}), and lower estuaries (S_P > 25) are weak sources (8.4 ± 14.3 mol C m^{-2} yr^{-1}). Predictably, with its maritime region occupying almost three-fourths of the total surface area, the SLE behaves like an outer estuary with only small CO_2 evasion. The lack of temporal coverage of surface-water pCO_2 data, however, prevents us from reliably synthesizing an annual air-sea CO_2 flux.

3.3. Major drivers of estuarine pCO_2 variability

The pCO_2 in the surface mixed layer is a function of its temperature (T), salinity (S_P), dissolved inorganic carbon (DIC) and total alkalinity (TAlk), as described by the following relationship (Takahashi et al., 1993):

$$dpCO_2 = (\partial pCO_2/\partial T)dT + (\partial pCO_2/\partial S_P)dS_P + (\partial pCO_2/\partial DIC)dDIC + (\partial pCO_2/\partial TAlk)dTAlk \quad (9)$$

Through changes in T, S_P, DIC and TAlk, variations of surface-water pCO_2 are mainly controlled by dynamic processes (water mass mixing), thermodynamic processes (temperature and salinity changes), air-sea gas exchange, and biological processes (photosynthesis, respiration) (Poisson et al., 1993). Among these, the effects of temperature and DIC, i.e., the addition or removal of DIC through biological activity and mixing processes, are generally the most important drivers of estuarine pCO_2 variability. In the absence of a significant source or sink of TAlk (e.g., calcium carbonate formation/dissolution, anaerobic organic matter decomposition), changes of DIC determine the buffer capacity (DIC/TAlk ratio) of the water. Whereas the physically and biologically induced changes of DIC/pCO_2 will be quantified in a future study, using a modified OMP water mass analysis, here, we evaluate the relative importance of thermal and biological processes in controlling the spatial distribution of pCO_2 in the St. Lawrence Estuary and Gulf.

To disentangle the biological and temperature effects on the spatial variability of pCO_2, the DO(% sat) were plotted against the pCO_2(% sat), with the origin at 100 % saturation for both gases. This simple approach uses the four possible combinations of pCO_2(% sat)/DO(% sat) as integrated measures of thermally and biologically induced changes. As shown in Fig. 8 (top), microbial respiration was the major driver of pCO_2 variability in the USLE, whereas photosynthesis and temperature were the dominant controls in the LSLE and GSL. We found similar results from a comparison of eDIC and AOU (Fig. 8, bottom). In the strongly stratified Lower Estuary, as well as near the estuary-gulf boundary, the biological drawdown of CO_2 counteracted the decrease in CO_2 gas solubility due to increasing temperature (Fig. 9). Its waters were mostly undersaturated with CO_2 with respect to the atmosphere (values of pCO_2 were below atmospheric level) despite a general trend of surface-water warming (T = 2.7 to 12.6

°C). This pattern is consistent with the finding that, in spring/summer, the increasing effect of warming on pCO_2 is counteracted by the photosynthetic utilization of CO_2, particularly in a strongly stratified shallow mixed layer (Takahashi et al., 1993). Whereas direct measurements of chlorophyll-a concentrations were not carried out during the research cruises, a fluorescence sensor was mounted on the CTD probe. As shown in Fig. 10, maximum fluorescence values, as well as high values of transmission (% light transmission approaching 100%), were observed in the eastern Lower Estuary and the western Gulf of St. Lawrence, where the system appears to shift from net heterotrophy to net autotrophy. Farther into the Gulf (near Anticosti Island), the temperature dependence of pCO_2 exerted a stronger influence, causing values of surface-water pCO_2 to increase concomitantly with temperature (Fig. 9).

4. Conclusions

Because of its large physical dimensions and unimpeded connection to the Atlantic Ocean, the St. Lawrence Estuary encompasses both a river-dominated inner estuary, where physical mixing and abiotic processes dominate, and a marine-dominated outer estuary, where biological cycling and oceanic processes prevail. The physical and biogeochemical processes of these contrasting environments are reflected in the spatial distribution of surface-water pCO_2 (139–765 µatm). The shallow, partially mixed Upper Estuary, with a turbidity maximum controlled by tide- and wind-induced turbulence, was, during our sampling period, a net source of CO_2 to the atmosphere due to microbial respiration (low biological productivity), whereas the deep, stratified Lower Estuary, with its stable, summertime three-layer vertical structure, was generally a net sink of atmospheric CO_2 due to the enhanced biological drawdown of pCO_2 (light availability, nutrient supply, strong stratification).

Overall, the large subarctic St. Lawrence Estuary was a weak source of CO_2 to the atmosphere, with an area-averaged CO_2 degassing flux of 0.98 to 2.02 mmol C m^{-2} d^{-1} (0.36 to 0.74 mol C m^{-2} yr^{-1}). This efflux is somewhat smaller than the numerically averaged CO_2 flux per unit area (2.19 mol C m^{-2} yr^{-1}) reported from North American estuaries by Chen et al. (2013), highlighting their relatively small contribution (~12 %) to global estuarine CO_2 emissions. The pronounced shift in source/sink dynamics in the St. Lawrence Estuary, between its river-dominated (9.2 ± 5.3 mmol m^{-2} d^{-1}) and

marine-dominated (0.8 ± 7.2 mmol m^{-2} d^{-1}) regions, is consistent with the conclusions of the comparative study carried out by Jiang et al. (2008) that revealed large differences in CO_2 degassing between riverine (inner) and maritime (outer) estuaries. Given the limited research on CO_2 dynamics in large estuaries and bay systems, which cover approximately one-half of the estuarine surface area on the U.S. east coast, as well as the large uncertainties in the indirect measurement of pCO_2 (carbonic acid dissociation constants, organic alkalinity contribution), current global-scale estimates of estuarine CO_2 degassing may be overestimated. To better constrain the role of large estuaries/bays in the coastal ocean carbon cycle, more extensive spatial and temporal coverage of direct pCO_2 measurements across estuary types is needed.

Data availability

Data presented in this paper (Figures 4 and 8) are available upon request from one of the authors (alfonso.mucci@mcgill.ca).

Author contribution

A.D. and A.M. conceived the project. A.M. acquired and processed the data prior to 2016. A.D. conducted the data analysis and wrote the first draft of the paper whereas A.M. provided editorial and scientific recommendations.

Competing interests

The authors declare that they have no conflict of interest.

Acknowledgements

We wish to thank the Captains and crews of the RV *Coriolis II* for their unwavering help over the years. We also wish to acknowledge Gilles Desmeules and Michel Rousseau for their dedicated electronic and field sampling support as well as Constance Guignard for her help in cruise preparation and field data acquisition. Most of the data acquisition was carried out opportunistically on research cruises funded by grants to A.M. or Canadian colleagues by the Natural Sciences and Engineering Research Council of Canada (NSERC) whereas the work was funded by a Regroupement Stratégique grant from the Fonds Québécois de Recherche Nature et Technologies (FQRNT) to GEOTOP as well as NSERC Discovery and MEOPAR grants to A.M. A.D. wishes to thank the Department of Earth and Planetary Sciences at McGill for financial support in the form of scholarships and assistantships.

References

751
752 Abril, G., Etcheber, H., Borges, A. V., and Frankignoulle, M.: Excess atmospheric carbon
753 dioxide transported by rivers into the Scheldt estuary, Cr. Acad. Sci. II A., 330, 761–768, 2000.
754
755 Abril, G., Commarieu, M. V., Sottolichio, A., Bretel, P., and Guerin, F.: Turbidity limits gas
756 exchange in a large macrotidal estuary, Estuar. Coast. Shelf Sci., 83, 342–348, 2009.
757
758 Abril, G. et al.: Technical Note: Large overestimation of pCO_2 calculated from pH and alkalinity
759 in acidic, organic-rich freshwaters, Biogeosciences, 12, 67–78, 2015.
760
761 Bauer, J. E., Cai, W. J., Raymond, P. A., Bianchi, T. S., Hopkinson, C. S., and Regnier, P. A.: The
762 changing carbon cycle of the coastal ocean, Nature, 504, 61–70, 2013.
763
764 Benson, B. B. and Krause, D.: The concentration and isotopic fractionation of oxygen dissolved
765 in freshwater and seawater in equilibrium with the atmosphere, Limnol. Oceanogr., 29, 620–
766 632, 1984.
767
768 Borges, A. V.: Do we have enough pieces of the jigsaw to integrate CO_2 fluxes in the coastal
769 ocean?, Estuaries, 28, 3–27, 2005.
770
771 Borges, A. V., and Abril, G.: Carbon dioxide and methane dynamics in estuaries, in: Wolanski,
772 E. and McLusky, D. S. (Eds.), Treatise on Estuarine and Coastal Science, Academic Press,
773 Waltham, 119–161, 2011.
774
775 Borges, A. V., Delille, B., Schiettecatte, L. S., Gazeau, F., Abril, G., and Frankignoulle, M.: Gas
776 transfer velocities of CO_2 in three European estuaries (Randers Fjord, Scheldt and Thames),
777 Limnol. Oceanogr., 49, 1630–1641, 2004a.
778
779 Borges, A. V., Vanderborght, J. P., Schiettecatte, L. S., Gazeau, F., Ferrón-Smith, S., Delille, B.,
780 and Frankignoulle, M.: Variability of the gas transfer velocity of CO_2 in a macrotidal estuary (the
781 Scheldt), Estuaries, 27, 593–603, 2004b.
782
783 Borges, A. V., Delille, B., and Frankignoulle, M.: Budgeting sinks and sources of CO_2 in the
784 coastal ocean: Diversity of ecosystems counts, Geophys. Res. Lett., 32, L14601,
785 doi:10.1029/2005GL023053, 2005.
786

Borges, A. V., Schiettecatte, L. S., Abril, G., Delille, B., and Gazeau, F.: Carbon dioxide in European coastal waters, Estuar. Coast. Shelf Sci., 70, 375–387, 2006.

Bugden, G. L.: Oceanographic conditions in the deeper waters of the Gulf of St. Lawrence in relation to local and oceanic forcing, NAFO SCR document 88/87, 1988.

Byrne, R. H.: Standardization of standard buffers by visible spectrometry, Anal. Chem., 59, 1479–1481, 1987.

Cai, W. J.: Estuarine and coastal ocean carbon paradox: CO_2 sinks or sites of terrestrial carbon incineration?, Annual Review of Marine Science, 3, 123–145, 2011.

Cai, W. J. and Wang, Y.: The chemistry, fluxes, and sources of carbon dioxide in the estuarine waters of the Satilla and Altamaha Rivers, Georgia, Limnol. Oceanogr., 43, 657–668, 1998.

Carrillo, C. J., Smith, R. C., and Karl, D. M.: Processes regulating oxygen and carbon dioxide in surface waters west of the Antarctic Peninsula, Mar. Chem., 84, 161–179, 2004.

Cerco, C. F.: Estimating estuarine reaeration rates, J. Environ. Eng.-ASCE, 115, 1066–1070, 1989.

Chen, C. T. A. and Borges, A. V.: Reconciling opposing views on carbon cycling in the coastal ocean: continental shelves as sinks and near-shore ecosystems as sources of atmospheric CO_2, Deep-Sea Res. Pt. II, 56, 578–590, 2009.

Chen, C. T. A., Huang, T. H., Fu, Y. H., Bai, Y., and He, X.: Strong sources of CO_2 in upper estuaries become sinks of CO_2 in large river plumes, Current Opinion in Environmental Sustainability, 4, 179–185, 2012.

Chen, C. T. A., Huang, T. H., Chen, Y. C., Bai, Y., He, X., and Kang, Y.: Air–sea exchanges of CO_2 in the world's coastal seas, Biogeosciences, 10, 6509–6544, 2013.

Clayton, T. D. and Byrne, R. H.: Spectrophotometric seawater pH measurements: total hydrogen ion concentration scale calibration of m-cresol purple and at-sea results, Deep-Sea Res. Pt. I, 40, 2115–2129, 1993.

Cloern, J. E.: Our evolving conceptual model of the coastal eutrophication problem, Mar. Ecol.-Prog. Ser., 210, 223–253, 2001.

Coote, A. R. and Yeats, P. A.: Distribution of nutrients in the Gulf of St. Lawrence, J. Fish. Res. Board Can., 36, 122–131, 1979.

Cotovicz Jr., L. C., Knoppers, B. A., Brandini, N., Costa Santos, S. J., and Abril, G.: A strong CO_2 sink enhanced by eutrophication in a tropical coastal embayment (Guanabara Bay, Rio de Janeiro, Brazil), Biogeosciences, 12, 6125–6146, 2015.

Cyr, F., Bourgault, D., Galbraith, P. S., and Gosselin, M.: Turbulent nitrate fluxes in the Lower St. Lawrence Estuary, Canada, J. Geophys. Res.-Oceans, 120, 2308–2330, 2015.

d'Anglejan, B.: Recent sediments and sediment transport processes in the St. Lawrence Estuary, in: El-Sabh, M. I. and Silverberg, N. (Eds.), Oceanography of a Large-scale Estuarine System, Springer-Verlag, New York, 109–129, 1990.

d'Anglejan, B. F. and Smith, E. C.: Distribution, transport, and composition of suspended matter in the St. Lawrence estuary, Can. J. Earth Sci., 10, 1380–1396, 1973.

de Boyer Montégut, C., Madec, G., Fischer, A. S., Lazar, A., and Iudicone, D.: Mixed layer depth over the global ocean: An examination of profile data and a profile-based climatology, J. Geophys. Res., 109, C12003, doi:10.1029/2004JC002378, 2004.

Dickson, A. G. and Goyet, C. (Eds.): Handbook of Methods for the Analysis of the Various Parameters of the Carbon Dioxide System in Sea Water (Version 2), U.S. Department of Energy, ORNL/CDIAC-74, 1994.

Dickson, A. G., Sabine, C. L., and Christian, J. R. (Eds.): Guide to Best Practices for Ocean CO_2 Measurements, PICES Special Publication 3, 191 pp., 2007.

Dufour, R. and Ouellet, P.: Estuary and Gulf of St. Lawrence marine ecosystem overview and assessment report, Can. Tech. Rep. Fish. Aquat. Sci., 2744E, 112 pp., 2007.

El-Sabh, M. I. and Murty, T. S.: Mathematical modelling of tides in the St. Lawrence Estuary, in: El-Sabh, M. I. and Silverberg, N. (Eds.), Oceanography of a Large-scale Estuarine System, Springer-Verlag, New York, 10–50, 1990.

El-Sabh, M. I. and Silverberg, N.: The St. Lawrence Estuary: introduction, in: El-Sabh, M. I. and Silverberg, N. (Eds.), Oceanography of a Large-scale Estuarine System, Springer-Verlag, New York, 1–9, 1990.

Frankignoulle, M. et al.: Carbon dioxide emission from European estuaries, Science, 282, 434–436, 1998.

Galbraith, P. S.: Winter water masses in the Gulf of St. Lawrence, J. Geophys. Res., 111, C06022, doi:10.1029/2005JC003159, 2006.

Gearing, J. N. and Pocklington, R.: Organic geochemical studies in the St. Lawrence Estuary, in: El-Sabh, M. I. and Silverberg, N. (Eds.), Oceanography of a Large-scale Estuarine System, Springer-Verlag, New York, 170–201, 1990.

Gilbert, D., Sundby, B., Gobeil, C., Mucci, A., and Tremblay, G. H.: A seventy-two-year record of diminishing deep-water oxygen in the St. Lawrence estuary: The northwest Atlantic connection, Limnol. Oceanogr., 50, 1654–1666, 2005.

Grasshoff, K., Kremling, K., and Ehrhardt, M. (Eds.): Methods of Seawater Analysis (3rd ed.), Wiley-VCH, Weinheim, Germany, 1999.

Gratton, Y., Mertz, G., and Gagné, J. A.: Satellite observations of tidal upwelling and mixing in the St. Lawrence Estuary, J. Geophys. Res.-Oceans, 93, 6947–6954, 1988.

Hélie, J. F. and Hillaire-Marcel, C.: Sources of particulate and dissolved organic carbon in the St Lawrence River: isotopic approach, Hydrol. Process., 20, 1945–1959, 2006.

Hélie, J. F., Hillaire-Marcel, C., and Rondeau, B.: Seasonal changes in the sources and fluxes of dissolved inorganic carbon through the St. Lawrence River—isotopic and chemical constraint, Chem. Geol., 186, 117–138, 2002.

Ho, D. T., Wanninkhof, R., Schlosser, P., Ullman, D. S., Hebert, D., and Sullivan, K. F.: Toward a universal relationship between wind speed and gas exchange: Gas transfer velocities measured with 3He/SF_6 during the Southern Ocean Gas Exchange Experiment, J. Geophys. Res., 116, C00F04, doi:10.1029/2010JC006854, 2011.

Hunt, C. W., Salisbury, J. E., and Vandemark, D.: Contribution of non-carbonate anions to total alkalinity and overestimation of pCO_2 in New England and New Brunswick rivers, Biogeosciences, 8, 3069–3076, 2011.

Ingram, R. G. and El-Sabh, M. I.: Fronts and mesoscale features in the St. Lawrence Estuary, in: El-Sabh, M. I. and Silverberg, N. (Eds.), Oceanography of a Large-scale Estuarine System, Springer-Verlag, New York, 71–93, 1990.

Jiang, L. Q., Cai, W. J., and Wang, Y.: A comparative study of carbon dioxide degassing in river- and marine-dominated estuaries, Limnol. Oceanogr., 53, 2603–2615, 2008.

Joesoef, A., Huang, W. J., Gao, Y., and Cai, W. J.: Air–water fluxes and sources of carbon dioxide in the Delaware Estuary: spatial and seasonal variability, Biogeosciences, 12, 6085–6101, 2015.

Kaul, L. W. and Froelich, P. N.: Modeling estuarine nutrient geochemistry in a simple system, Geochim. Cosmochim. Acta, 48, 1417–1433, 1984.

Koné, Y. J. M., Abril, G., Kouadio, K. N., Delille, B., and Borges, A. V.: Seasonal variability of carbon dioxide in the rivers and lagoons of Ivory Coast (West Africa), Estuaries and Coasts, 32, 246–260, 2009.

Larouche, P., Koutitonsky, V. G., Chanut, J. P., and El-Sabh, M. I.: Lateral stratification and dynamic balance at the Matane transect in the lower Saint Lawrence estuary, Estuar. Coast. Shelf Sci., 24, 859–871, 1987.

Laruelle, G. G., Dürr, H. H., Slomp, C. P., and Borges, A. V.: Evaluation of sinks and sources of CO_2 in the global coastal ocean using a spatially-explicit typology of estuaries and continental shelves, Geophys. Res. Lett., 37, L15607, doi:10.1029/2010GL043691, 2010.

Laruelle, G. G., Dürr, H. H., Lauerwald, R., Hartmann, J., Slomp, C. P., Goossens, N., and Regnier, P. A. G.: Global multi-scale segmentation of continental and coastal waters from the watersheds to the continental margins, Hydrol. Earth Syst. Sci., 17, 2029–2051, 2013.

Laruelle, G. G., Lauerwald, R., Rotschi, J., Raymond, P. A., Hartmann, J., and Regnier, P.: Seasonal response of air-water CO_2 exchange along the land-ocean aquatic continuum of the northeast North American coast, Biogeosciences, 12, 1447–1458, 2015.

Lucotte, M.: Organic carbon isotope ratios and implications for the maximum turbidity zone of the St Lawrence upper estuary, Estuar. Coast. Shelf Sci., 29, 293–304, 1989.

Lucotte, M. and d'Anglejan, B.: Seasonal control of the Saint-Lawrence maximum turbidity zone by tidal-flat sedimentation, Estuaries, 9, 84–94, 1986.

Lucotte, M., Hillaire-Marcel, C., and Louchouarn, P.: First-order organic carbon budget in the St Lawrence Lower Estuary from ^{13}C data, Estuar. Coast. Shelf Sci., 32, 297–312, 1991.

Lueker, T. J., Dickson, A. G., and Keeling, C. D.: Ocean pCO_2 calculated from dissolved inorganic carbon, alkalinity, and equations for K_1 and K_2: validation based on laboratory measurements of CO_2 in gas and seawater at equilibrium, Mar. Chem., 70, 105–119, 2000.

Maher, D. T., and Eyre, B. D.: Carbon budgets for three autotrophic Australian estuaries: Implications for global estimates of the coastal air-water CO_2 flux, Global Biogeochem. Cycles, 26, GB1032, doi:10.1029/2011GB004075, 2012.

McDougall, T. J. and Barker, P. M.: Getting started with TEOS-10 and the Gibbs Seawater (GSW) Oceanographic Toolbox, SCOR/IAPSO WG127, ISBN 978-0-646-55621-5, 28 pp., 2011.

Mertz, G. and Gratton, Y.: Topographic waves and topographically induced motions in the St. Lawrence Estuary, in: El-Sabh, M. I. and Silverberg, N. (Eds.), Oceanography of a Large-scale Estuarine System, Springer-Verlag, New York, 94–108, 1990.

Middelburg, J. J. and Herman, P. M.: Organic matter processing in tidal estuaries, Mar. Chem., 106, 127–147, 2007.

Millero, F. J.: The thermodynamics of the carbonate system in seawater, Geochim. Cosmochim. Acta, 43, 1651–1661, 1979.

Millero, F. J.: The pH of estuarine waters, Limnol. Oceanogr., 31, 839–847, 1986.

Millero, F. J.: Carbonate constants for estuarine waters, Mar. Freshwater Res., 61, 139–142, 2010.

970 Monbet, Y.: Control of phytoplankton biomass in estuaries: a comparative analysis of microtidal
971 and macrotidal estuaries, Estuaries, 15, 563–571, 1992.
972
973 Mucci, A., Levasseur, M., Gratton, Y., Martias, C., Scarratt, M., Gilbert, D., Tremblay, J.-É.,
974 Ferreya, G., and Lansard, B.: Tidal-induced variations of pH at the head of the Laurentian
975 Channel, Can. J. Fish. Aquat. Sci. (in revision), 2016.
976
977 Orr, J. C., Epitalon, J. M., and Gattuso, J. P.: Comparison of ten packages that compute ocean
978 carbonate chemistry, Biogeosciences, 12, 1483–1510, 2015.
979
980 Painchaud, J. and Therriault, J. C.: Relationships between bacteria, phytoplankton and
981 particulate organic carbon in the upper St. Lawrence estuary, Mar. Ecol.-Prog. Ser., 56, 301–
982 311, 1989.
983
984 Painchaud, J., Lefaivre, D., Therriault, J. C., and Legendre, L.: Physical processes controlling
985 bacterial distribution and variability in the upper St. Lawrence estuary, Estuaries, 18, 433–444,
986 1995.
987
988 Pelletier, E. and Lebel, J.: Hydrochemistry of dissolved inorganic carbon in the St. Lawrence
989 Estuary (Canada), Estuar. Coast. Mar. Sci., 9, 785–795, 1979.
990
991 Peng, T. H., Takahashi, T., Broecker, W. S., and Olafsson, J.: Seasonal variability of carbon
992 dioxide, nutrients and oxygen in the northern North Atlantic surface water: observations and a
993 model, Tellus, 39B, 439–458, 1987.
994
995 Plourde, S. and Runge, J. A.: Reproduction of the planktonic copepod Calanus finmarchicus in
996 the Lower St. Lawrence Estuary: relation to the cycle of phytoplankton production and
997 evidence for a Calanus pump, Mar. Ecol.-Prog. Ser., 102, 217–227, 1993.
998
999 Pocklington, R. and Leonard, J. D.: Terrigenous organic matter in sediments of the St. Lawrence
1000 Estuary and the Saguenay Fjord, J. Fish. Res. Board Can., 36, 1250–1255, 1979.
1001
1002 Poisson, A., Metzl, N., Brunet, C., Schauer, B., Bres, B., Ruiz-Pino, D., and Louanchi, F.: Variability
1003 of sources and sinks of CO_2 in the Western Indian and Southern Oceans during the year 1991,
1004 J. Geophys. Res.-Oceans, 98, 22759–22778, 1993.
1005

1006 Raymond, P. A. and Cole, J. J.: Gas exchange in rivers and estuaries: Choosing a gas transfer
1007 velocity, Estuaries, 24, 312–317, 2001.
1008
1009 Raymond, P. A., Bauer, J. E., and Cole, J. J.: Atmospheric CO_2 evasion, dissolved inorganic
1010 carbon production, and net heterotrophy in the York River estuary, Limnol. Oceanogr., 45,
1011 1707–1717, 2000.
1012
1013 Regnier, P. et al.: Anthropogenic perturbation of the carbon fluxes from land to ocean, Nat.
1014 Geosci., 6, 597–607, 2013.
1015
1016 Richey, J. E., Devol, A. H., Wofsy, S. C., Victoria, R., and Riberio, M. N.: Biogenic gases and the
1017 oxidation and reduction of carbon in Amazon River and floodplain waters, Limnol. Oceanogr.,
1018 33, 551–561, 1988.
1019
1020 Robert-Baldo, G. L., Morris, M. J., and Byrne, R. H.: Spectrophotometric determination of
1021 seawater pH using phenol red, Anal. Chem., 57, 2564–2567, 1985.
1022
1023 Roy, R. N. et al.: The dissociation constants of carbonic acid in seawater at salinities 5 to 45 and
1024 temperatures 0 to 45°C, Mar. Chem., 44, 249–267, 1993.
1025
1026 Saucier, F. J. and Chassé, J.: Tidal circulation and buoyancy effects in the St. Lawrence Estuary,
1027 Atmos. Ocean, 38, 505–556, 2000.
1028
1029 Saucier, F. J., Roy, F., Gilbert, D., Pellerin, P., and Ritchie, H.: Modeling the formation and
1030 circulation processes of water masses and sea ice in the Gulf of St. Lawrence, Canada. J.
1031 Geophys. Res., 108, 3269, doi:10.1029/2000JC000686, 2003.
1032
1033 Savenkoff, C., Comeau, L., Vézina, A. F., and Gratton, Y.: Seasonal variation of the biological
1034 activity in the lower St. Lawrence Estuary, Can. Tech. Rep. Fish. Aquat. Sci., 2006, 22 pp., 1994.
1035
1036 Silverberg, N. and Sundby, B.: Observations in the turbidity maximum of the St. Lawrence
1037 estuary, Can. J. Earth Sci., 16, 939–950, 1979.
1038
1039 Sprintall, J. and Tomczak, M.: Evidence of the barrier layer in the surface layer of the tropics, J.
1040 Geophys. Res.-Oceans, 97, 7305–7316, 1992.
1041

Statham, P. J.: Nutrients in estuaries—an overview and the potential impacts of climate change, Sci. Total Environ., 434, 213–227, 2012.

Takahashi, T., Olafsson, J., Goddard, J. G., Chipman, D. W., and Sutherland, S. C.: Seasonal variation of CO_2 and nutrients in the high-latitude surface oceans: a comparative study, Global Biogeochem. Cycles, 7, 843–878, 1993.

Takahashi, T. et al.: Global sea–air CO_2 flux based on climatological surface ocean pCO_2, and seasonal biological and temperature effects, Deep-Sea Res. Pt. II, 49, 1601–1622, 2002.

Tan, F. C. and Strain, P. M.: Sources, sinks and distribution of organic carbon in the St. Lawrence Estuary, Canada, Geochim. Cosmochim. Acta, 47, 125–132, 1983.

Tee, K-T.: Meteorologically and buoyancy induced subtidal salinity and velocity variations in the St. Lawrence Estuary, in: El-Sabh, M. I. and Silverberg, N. (Eds.), Oceanography of a Large-scale Estuarine System, Springer-Verlag, New York, 51–70, 1990.

Uncles, R. J., Stephens, J. A., and Smith, R. E.: The dependence of estuarine turbidity on tidal intrusion length, tidal range and residence time, Cont. Shelf Res., 22, 1835–1856, 2002.

van Heuven, S., Pierrot, D., Rae, J. W. B., Lewis, E., and Wallace, D. W. R.: MATLAB program developed for CO_2 system calculations, ORNL/CDIAC-105b, Carbon Dioxide Information Analysis Center, Oak Ridge National Laboratory, U.S. Department of Energy, Oak Ridge, Tennessee, doi: 10.3334/CDIAC/otg.CO2SYS_MATLAB_v1.1, 2011.

Wanninkhof, R.: Relationship between wind speed and gas exchange over the ocean, J. Geophys. Res.-Oceans, 97, 7373–7382, 1992.

Wanninkhof, R.: Relationship between wind speed and gas exchange over the ocean revisited, Limnol. Oceanogr.–Meth., 12, 351–362, 2014.

Weiss, R.: Carbon dioxide in water and seawater: the solubility of a non-ideal gas, Mar. Chem., 2, 203–215, 1974.

Weiss, R. F. and Price, B. A.: Nitrous oxide solubility in water and seawater, Mar. Chem., 8, 347–359, 1980.

Working Group on the State of the St. Lawrence Monitoring, Overview of the State of the St. Lawrence 2014, St. Lawrence Action Plan, Environment Canada, Québec's ministère du Développement durable, de l'Environnement et de la Lutte contre les changements climatiques), Québec's ministère des Forêts, de la Faune et des Parcs, Parks Canada, Fisheries and Oceans Canada, and Stratégies Saint‐Laurent, 52 pp., 2014.

Yang, B., Byrne, R. H., and Lindemuth, M.: Contributions of organic alkalinity to total alkalinity in coastal waters: A spectrophotometric approach, Mar. Chem., 176, 199–207, 2015.

Yang, C., Telmer, K., and Veizer, J.: Chemical dynamics of the "St. Lawrence" riverine system: δD_{H2O}, $\delta^{18}O_{H2O}$, $\delta^{13}C_{DIC}$, $\delta^{34}S_{sulfate}$, and dissolved $^{87}Sr/^{86}Sr$, Geochim. Cosmochim. Acta, 60, 851–866, 1996.

Yeats, P. A.: Reactivity and transport of nutrients and metals in the St. Lawrence Estuary, in: El-Sabh, M. I. and Silverberg, N. (Eds.), Oceanography of a Large-scale Estuarine System, Springer-Verlag, New York, 155–169, 1990.

Zakardjian, B. A., Gratton, Y., and Vézina, A. F.: Late spring phytoplankton bloom in the Lower St. Lawrence Estuary: the flushing hypothesis revisited, Mar. Ecol.-Prog. Ser., 192, 31–48, 2000.

Zappa, C. J., Raymond, P. A., Terray, E. A., and McGillis, W. R.: Variation in surface turbulence and the gas transfer velocity over a tidal cycle in a macro-tidal estuary, Estuaries, 26, 1401–1415, 2003.

Zappa, C. J., McGillis, W. R., Raymond, P. A., Edson, J. B., Hintsa, E. J., Zemmelink, H. J., Dacey, J. W. H., and Ho, D. T.: Environmental turbulent mixing controls on air-water gas exchange in marine and aquatic systems, Geophys. Res. Lett., 34, L10601, doi:10.1029/2006GL028790, 2007.

Table 1. Mean, standard deviation and range of the surface-water temperature (T), practical salinity (S_P), dissolved inorganic carbon (DIC), total alkalinity (TAlk) and *in situ* partial pressure of CO_2 (pCO_2) in the St. Lawrence River (near Québec City), Upper Estuary (Île d'Orléans to Tadoussac), Lower Estuary (Tadoussac to Pointe-des-Monts) and Gulf (Pointe-des-Monts to Cabot Strait) during all sampling months.

	T (°C)	S_P	DIC (μmol kg^{-1})	TAlk (μmol kg^{-1})	pCO_2 (μatm)
River (N=3)	14.2 ± 3.9 (9.8–17.2)	0.03 ± 0.05 (0–0.09)	1242 ± 132 (1148–1335)	1204 ± 99 (1124–1314)	604 ± 76 (550–658)
Upper (N=46)	9.6 ± 3.6 (4.2–17.4)	10.9 ± 8.0 (0–24.5)	1514 ± 242 (1081–2005)	1492 ± 272 (969–2030)	571 ± 72 (435–765)
Lower (N=60)	6.2 ± 2.2 (2.7–12.6)	26.2 ± 2.1 (21.2–30.4)	1837 ± 82 (1634–2005)	1957 ± 82 (1752–2088)	394 ± 119 (139–578)
Gulf (N=30)	8.8 ± 3.1 (3.9–13.7)	30.1 ± 1.5 (25.5–31.5)	1936 ± 64 (1761–2032)	2096 ± 61 (1921–2175)	352 ± 80 (207–478)

Table 2. Mean, standard deviation and range of ΔpCO_2, k_{W-14}, $k_{R\&C-01}$, F_{W-14} and $F_{R\&C-01}$ in the surface waters of the St. Lawrence River, Upper Estuary, Lower Estuary and Gulf during all sampling months. k_{W-14} are the gas transfer velocities given by the Wanninkhof (2014) relationship, whereas $k_{R\&C-01}$ are those given by Raymond and Cole (2001). Values of F_{W-14} are taken to be the theoretical lower limit of air-sea gas exchange, whereas values of $F_{R\&C-01}$ are the upper limit; the extreme F data points are shown in bold.

	ΔpCO_2 (µatm)	k_{W-14} (cm h^{-1})	$k_{R\&C-01}$ (cm h^{-1})	F_{W-14} (mmol m^{-2} d^{-1})	$F_{R\&C-01}$ (mmol m^{-2} d^{-1})
River (N=3)	217 ± 99 (147–287)	3.0 ± 1.4 (1.9–4.5)	6.1 ± 2.0 (4.3–8.2)	5.8 ± 3.2 (**3.5**–8.0)	12.7 ± 6.4 (8.2–**17.3**)
Upper (N=46)	184 ± 72 (43–386)	2.8 ± 0.8 (1.6–4.5)	5.6 ± 1.1 (3.8–8.1)	6.1 ± 3.0 (**2.0**–14.7)	12.3 ± 5.4 (3.6–**28.4**)
Lower (N=60)	9.2 ± 116 (–266–188)	3.2 ± 0.4 (2.0–3.8)	5.9 ± 0.6 (4.3–6.9)	0.6 ± 4.9 (–12.1–8.3)	1.0 ± 9.0 (**–21.9**–**15.1**)
Gulf (N=30)	–31.0 ± 90 (–178–107)	1.2 ± 0.3 (0.8–1.7)	3.4 ± 0.3 (2.8–4.1)	–0.8 ± 1.5 (–3.6–1.1)	–1.7 ± 3.9 (**–8.4**–**3.6**)

Table 3. Sectional and area-averaged air-sea CO_2 fluxes (mmol C m^{-2} d^{-1}) in the St. Lawrence Estuary during all sampling months. To obtain the area-averaged CO_2 flux, the SLE was divided into five segments at equal intervals. The first row of the table shows the surface area (km^2) of each segment. The flux data in each segment were numerically averaged to obtain sectional fluxes, which were then area weighted and summed to obtain the spatially integrated whole-estuary flux (in bold). The $F_{W\text{-}14}$ and $F_{R\&C\text{-}01}$ data provide the lower and upper estimates, respectively.

	Seg 1 (N=17)	Seg 2 (N=23)	Seg 3 (N=21)	Seg 4 (N=17)	Seg 5 (N=8)	Whole estuary
Surface area (km^2)	1,098	2,250	2,726	3,404	3,303	12,781
$F_{W\text{-}14}$ (mmol m^{-2} d^{-1})	7.2	5.4	4.3	–1.8	–4.0	**0.98**
$F_{R\&C\text{-}01}$ (mmol m^{-2} d^{-1})	14.5	11.0	7.9	–3.5	–7.4	**2.02**

Figure 1. Map of the greater St. Lawrence system, including the chain of Great Lakes, the St. Lawrence River, the Upper St. Lawrence Estuary (USLE), the Lower St. Lawrence Estuary (LSLE), and the Gulf of St. Lawrence (GSL). From: Overview of the State of the St. Lawrence 2014 (with permission).

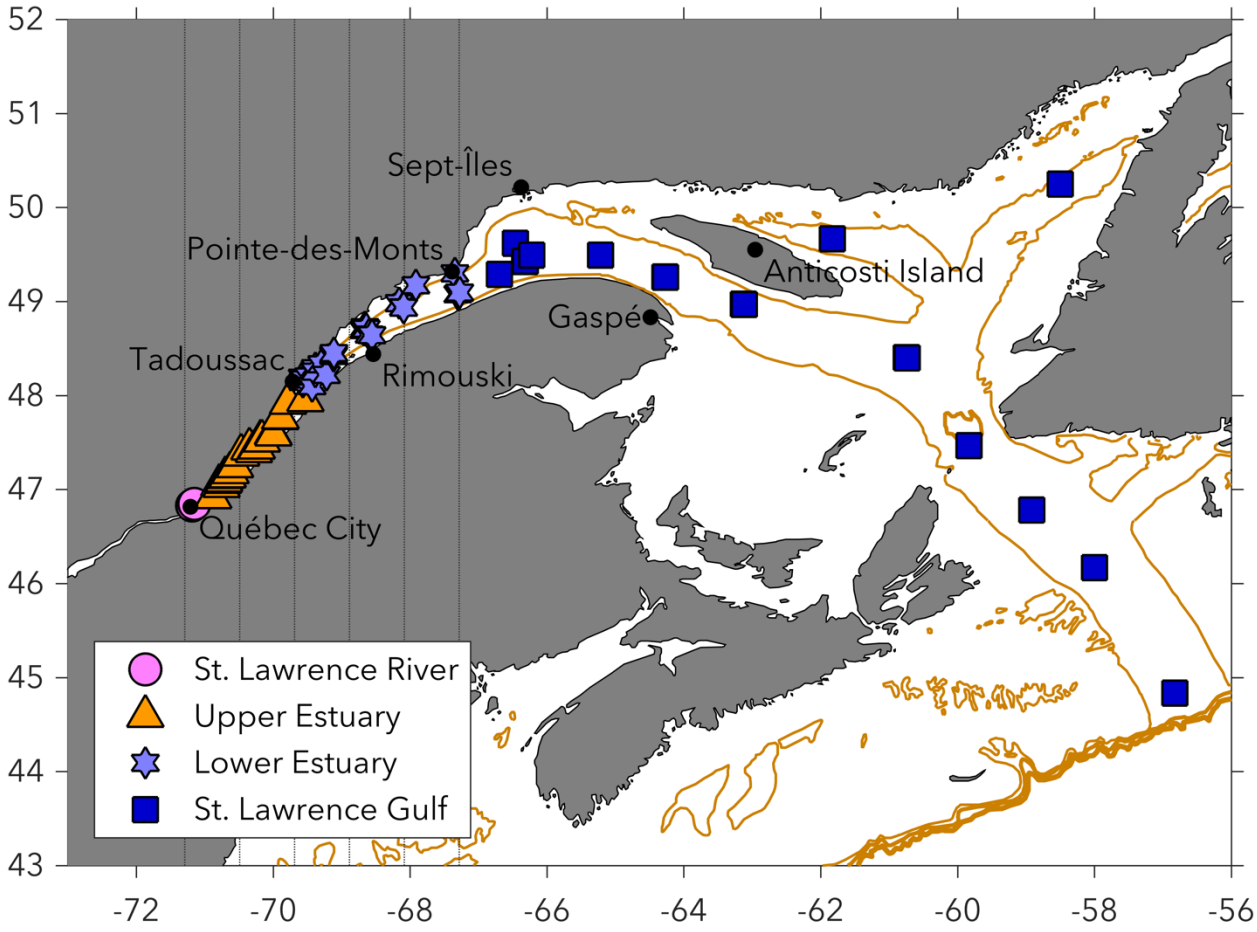

Figure 2. Map showing the four principal subdivisions of the study area and the sampling locations (markers). Water samples were collected during ten spring/summer research cruises: July 2003, June 2006, May 2007, July 2007, June 2009, July 2009, July 2010, May 2011, June 2013 and May 2016. The estuary, from the landward limit of the salt water intrusion near Île d'Orléans (~5 km downstream of Québec City) to Pointe-des-Monts, where the coastline diverges, extends ~400 km and covers a total surface area of ~12,820 km^2. The solid gold line follows the 200m isobath of the Laurentian Channel. The vertical dotted lines delineate the five segments of the estuary used for the calculation of the area-averaged CO_2 flux.

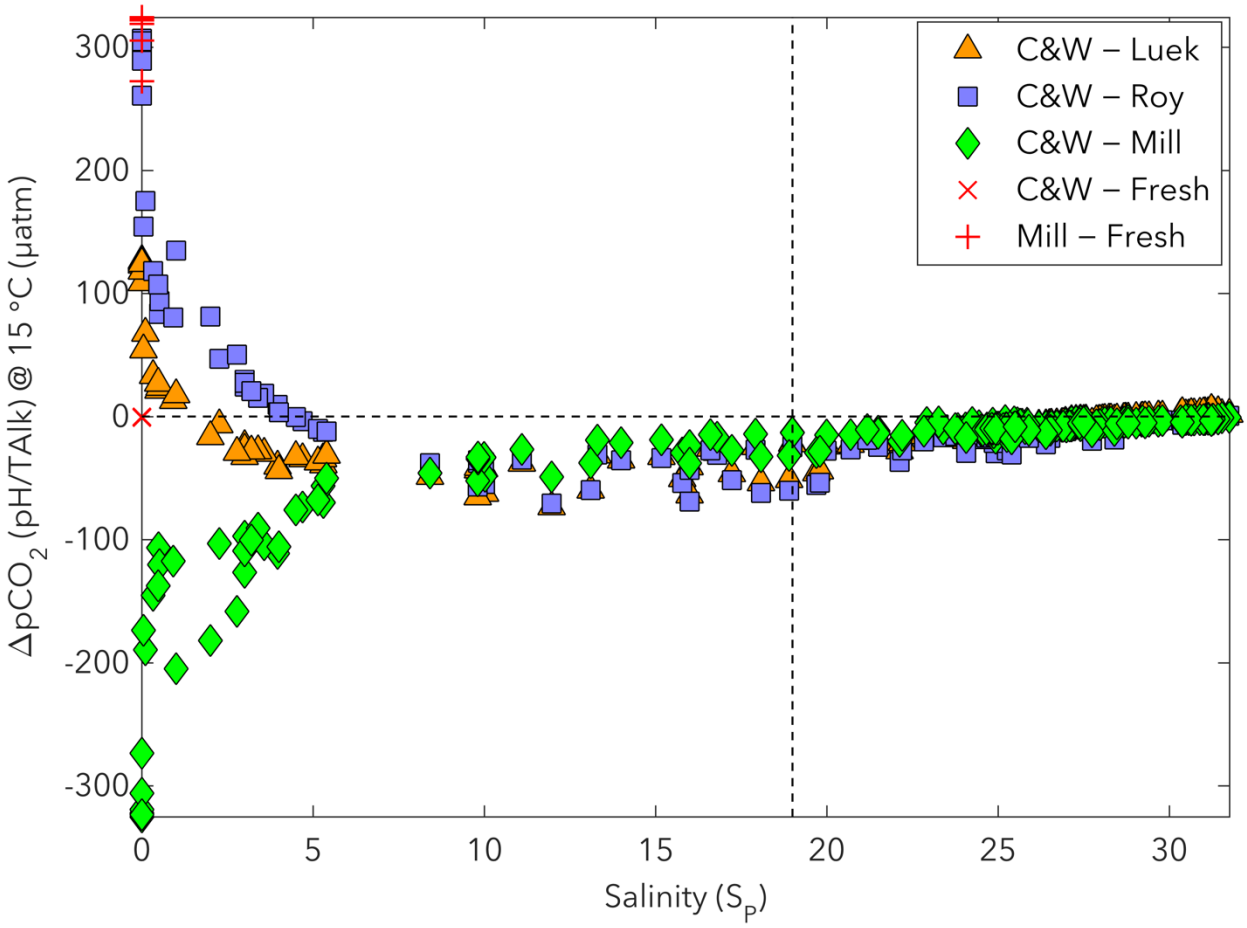

Figure 3. Differences in pCO_2 (ΔpCO_2) calculated using different published formulations of K_1 and K_2, including Cai and Wang (1998) [C&W], Lueker et al. (2000) [Luek], Roy et al. (1993) [Roy], Millero (2010) [Mill], and Millero (1979) for pure water only (S_P = 0) [Fresh]. All calculations were carried out at 15 °C (pCO_2 @ 15 °C) with measured pH and TAlk. The constants of Lueker et al. (2000) are recommended for best practices by Dickson et al. (2007), whereas those of Roy et al. (1993) (S_P = 5 to 45) are recommended by Dickson and Goyet (1994). Both the constants of Cai and Wang (1998) and Millero (2010) have been proposed as more appropriate for the study of the carbonate system in estuarine waters.

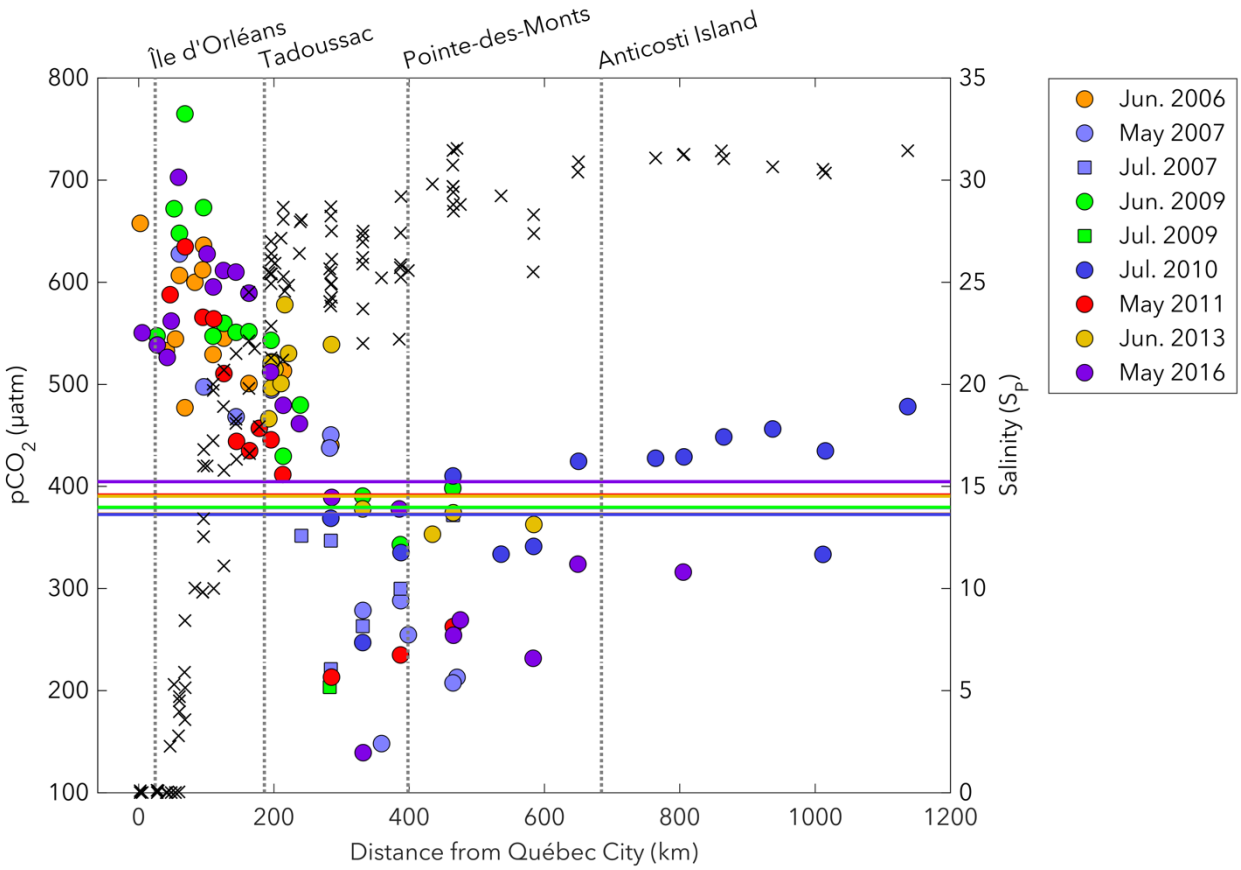

Figure 4. Spatial distributions of surface-water pCO_2 (circles, squares) and practical salinity (x symbols) in the St. Lawrence River, Estuary and Gulf during spring/summer cruises. Horizontal lines show the mean pCO_2(air) in the sampling months. The pCO_2 data points above atmospheric level are sources of CO_2 to the atmosphere whereas those below atmospheric level are sinks of atmospheric CO_2.

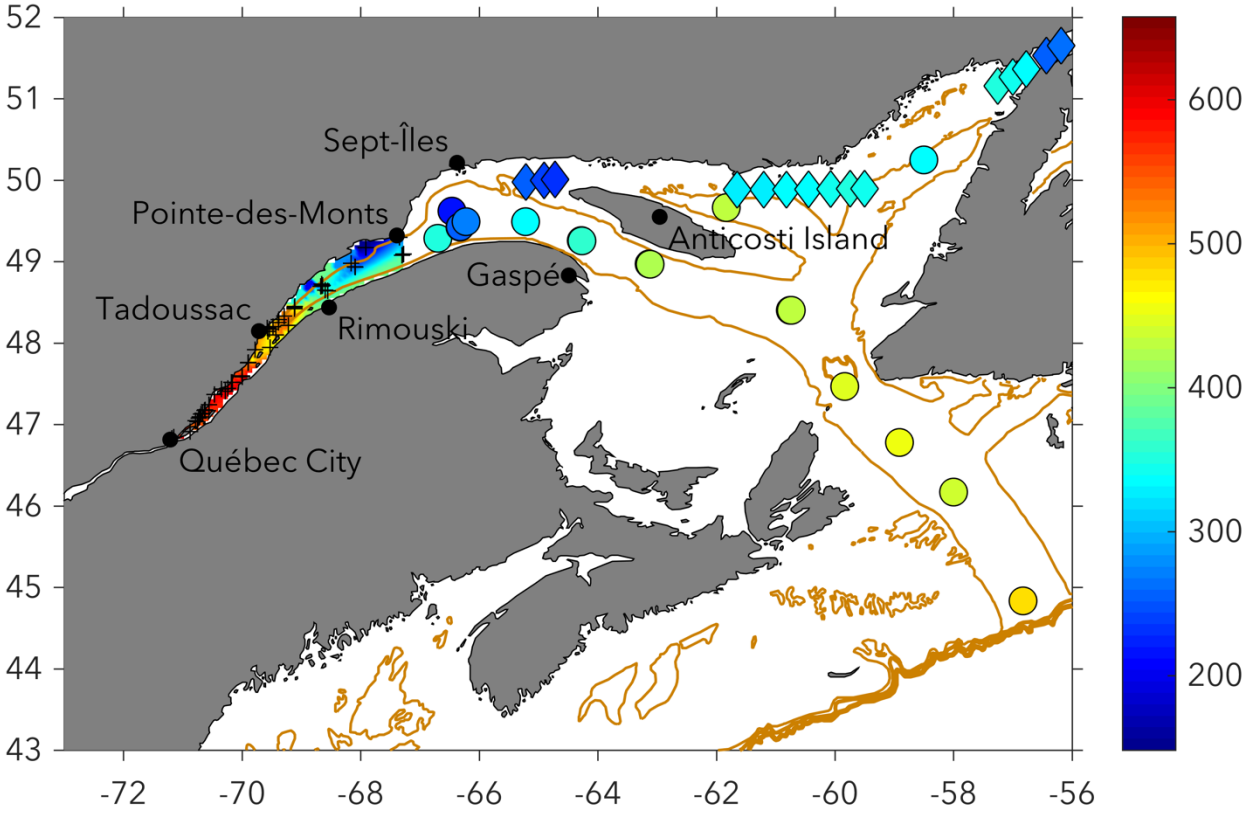

Figure 5. Spatial distribution of surface-water pCO_2 (µatm) in the St. Lawrence Estuary and Gulf during all spring/summer cruises. Linear interpolation was used between the sampling locations in the estuary (+ symbols). Circles show calculated pCO_2 (pH/TAlk), whereas diamonds show pCO_2 measured by the underway system (General Oceanics model 8050) aboard the CCGS *Amundsen* in June 2016 (Dr. Tim Papakyriakou/University of Manitoba, pers. comm.). For neighboring locations sampled in May 2016 aboard the RV *Coriolis II*, measured and calculated pCO_2 differed by, on average, ~4.2 %. The mean atmospheric pCO_2 during the sampling months ranged from 372 to 405 µatm.

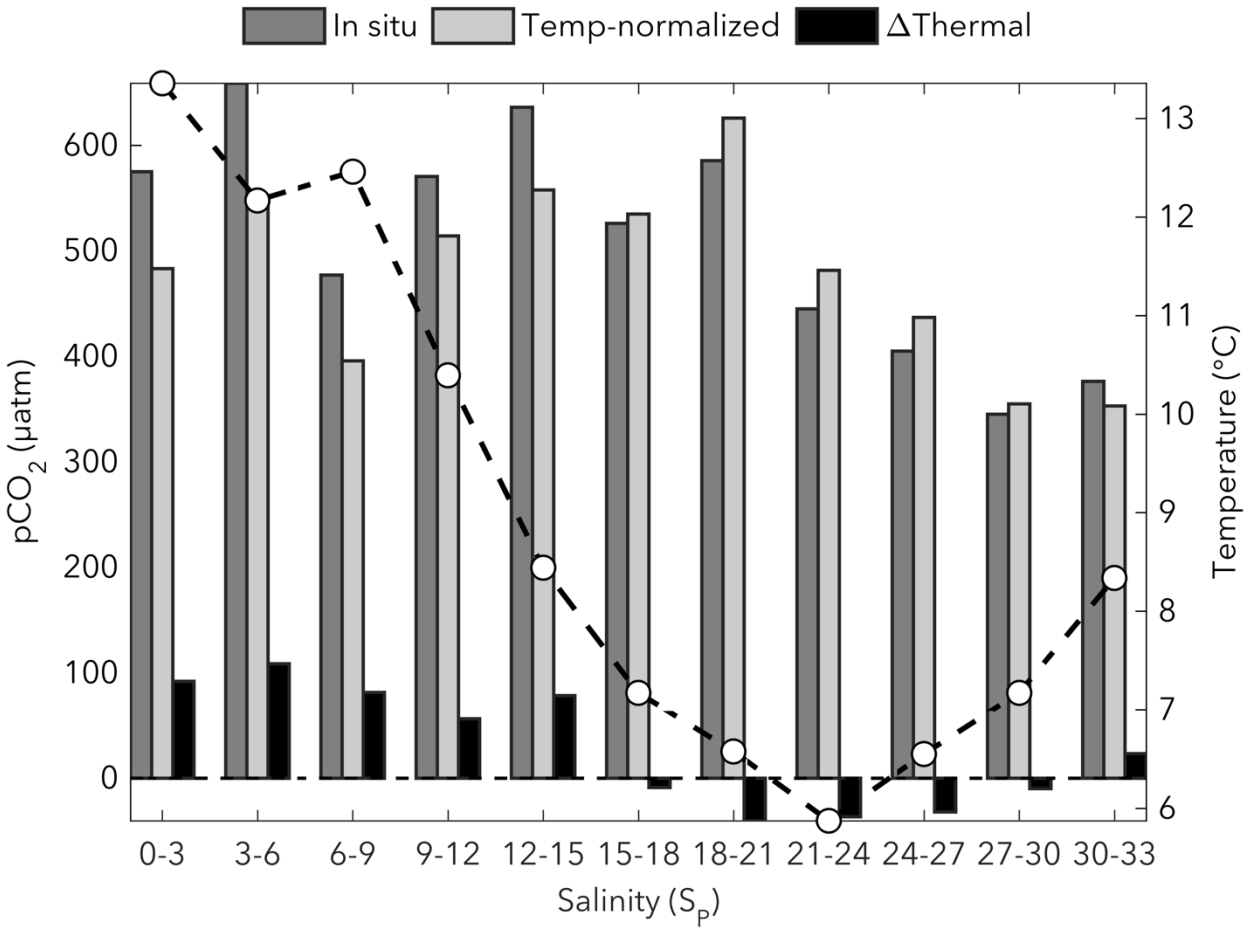

Figure 6. Surface-water *in situ* pCO_2, temperature-normalized pCO_2, and ΔpCO_2(temp) averaged over salinity bins of 3. The open circles show the average temperature for each salinity bin. To correct for the increasing/decreasing effect of temperature on surface-water pCO_2, the *in situ* pCO_2 were normalized to the average surface-water temperature of the study area (T = 7.82 °C). The ΔpCO_2(temp) are the thermally-induced pCO_2 changes due to temperature deviations from T = 7.82 °C, whereas variations in temperature-normalized pCO_2 are due to water mass mixing and/or biological activity.

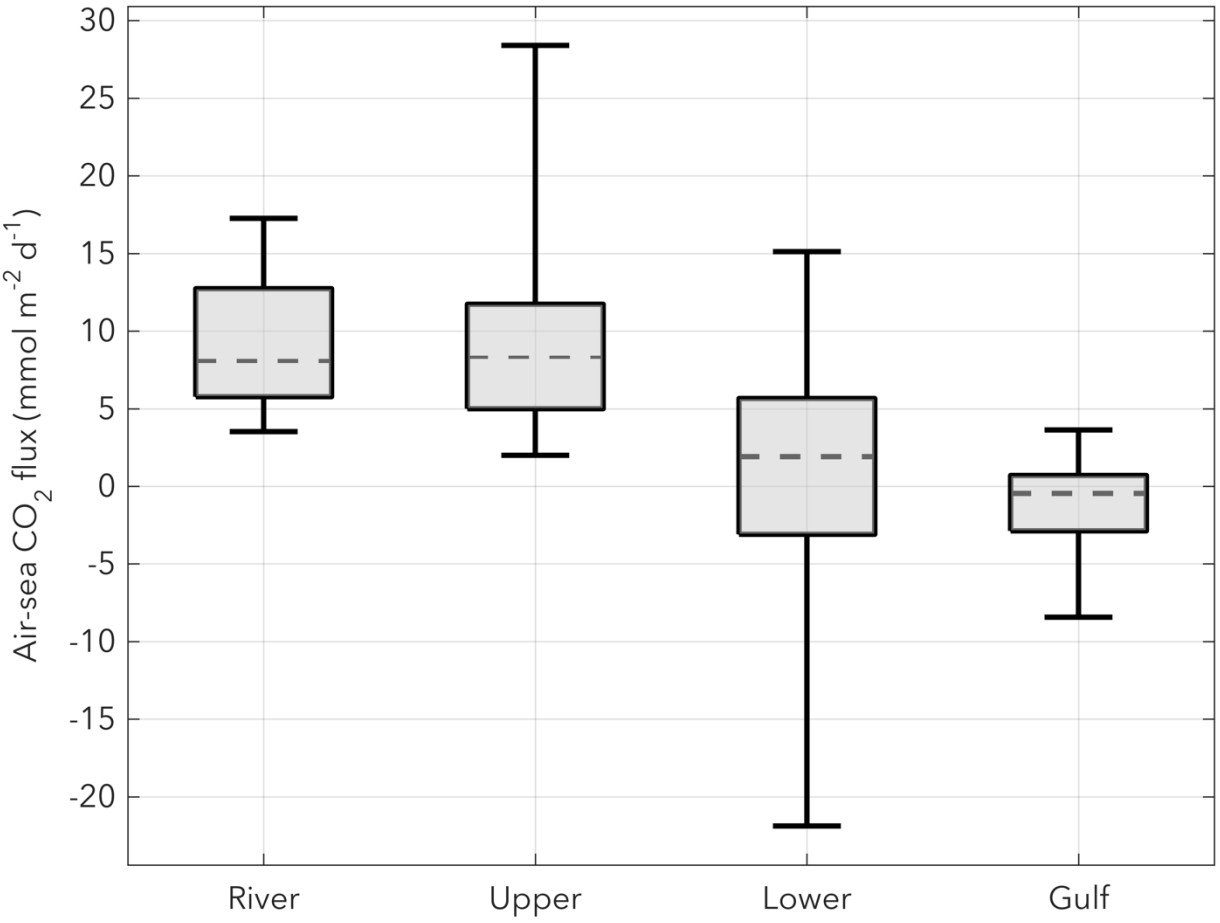

Figure 7. Box plot showing the variability of air-sea CO_2 fluxes in the four principal subdivisions of the study area (St. Lawrence River, Upper Estuary, Lower Estuary and Gulf). The box spans the interquartile range (25–75 percentiles), the dashed line is the median, and the whiskers extend to the extreme data points. The $F_{W\text{-}14}$ data were combined with the $F_{R\&C\text{-}01}$ data from all spring/summer sampling months to depict the upper and lower limits of gas exchange.

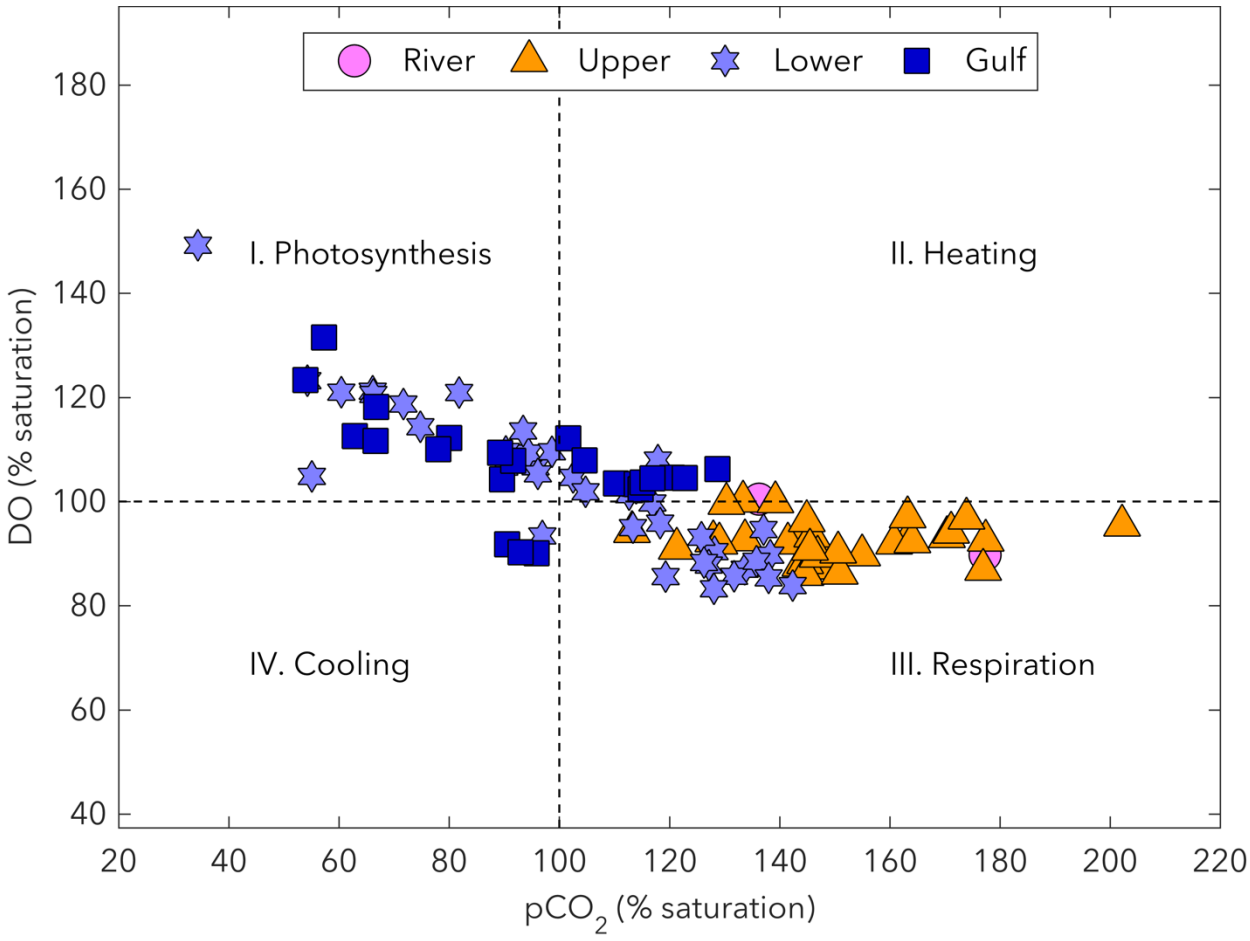
River
Upper
Lower
Gulf
I. Photosynthesis
II. Heating
III. Respiration
IV. Cooling
DO (% saturation)
pCO2 (% saturation)
180
160
140
120
100
80
60
40
20
40
60
80
100
120
140
160
180
200
220

1308

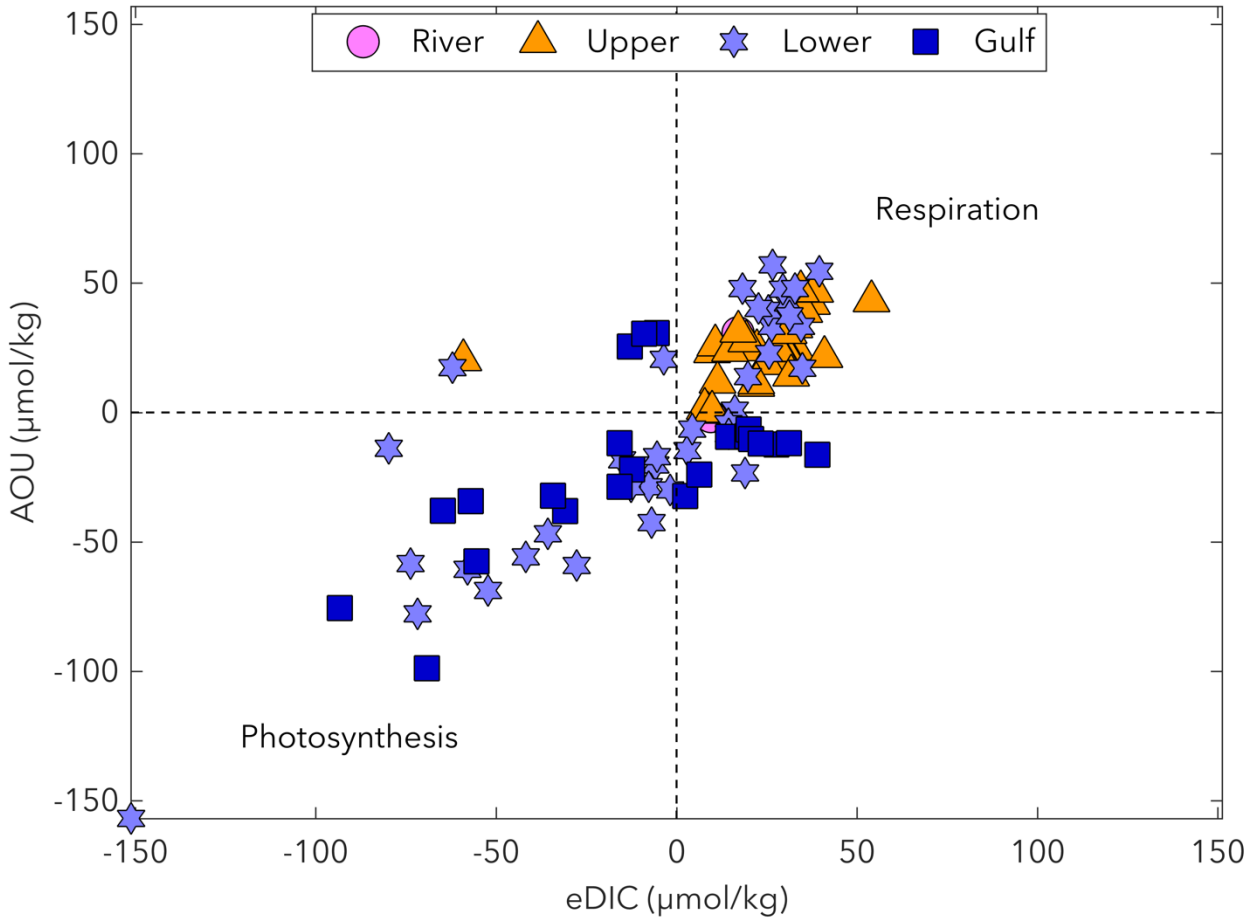

Figure 8. Top: comparison of the saturation states (or % saturation) of pCO_2 and DO in the mixed-layer waters of the St. Lawrence River, Estuary and Gulf. Dashed lines delineate the 100 % saturation levels for both gases. Surface-water samples (markers) fall into one of four quadrants representing the dominant controls on CO_2/O_2 dynamics. Quadrants I and III indicate the effects of photosynthesis/respiration, whereas Quadrants II and IV indicate heating/cooling. Bottom: comparison of the apparent oxygen utilization (AOU) and excess DIC (eDIC). Respiration/remineralization processes are reflected in positive values of AOU and eDIC, whereas the effects of photosynthesis are reflected in negative values.

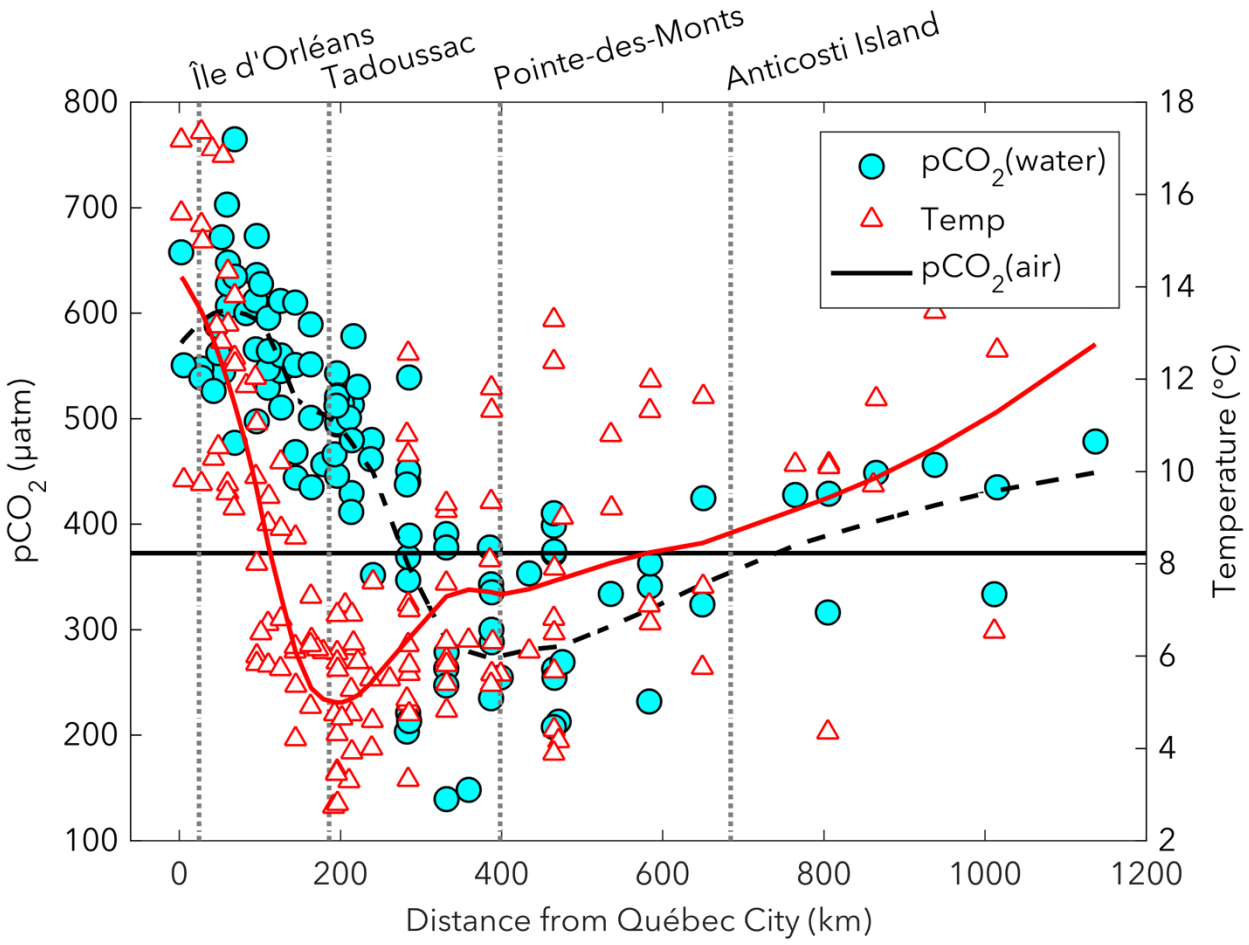

Figure 9. Spatial distributions of surface-water pCO_2 (circles) and temperature (triangles) in the St. Lawrence River, Estuary and Gulf during spring/summer cruises. Temperatures ranged from 4.2 to 17.4 °C (generally decreasing) in the USLE, 2.7 to 12.6 °C (generally increasing) in the LSLE, and 3.9 to 13.7 °C (generally increasing) in the GSL. The horizontal line shows the mean atmospheric pCO_2, pCO_2(air), during all sampling months. The dashed line is the smoothed pCO_2(water) data using a moving average filter with a span of 50% of the total number of data points, whereas the red line is the smoothed temperature data.

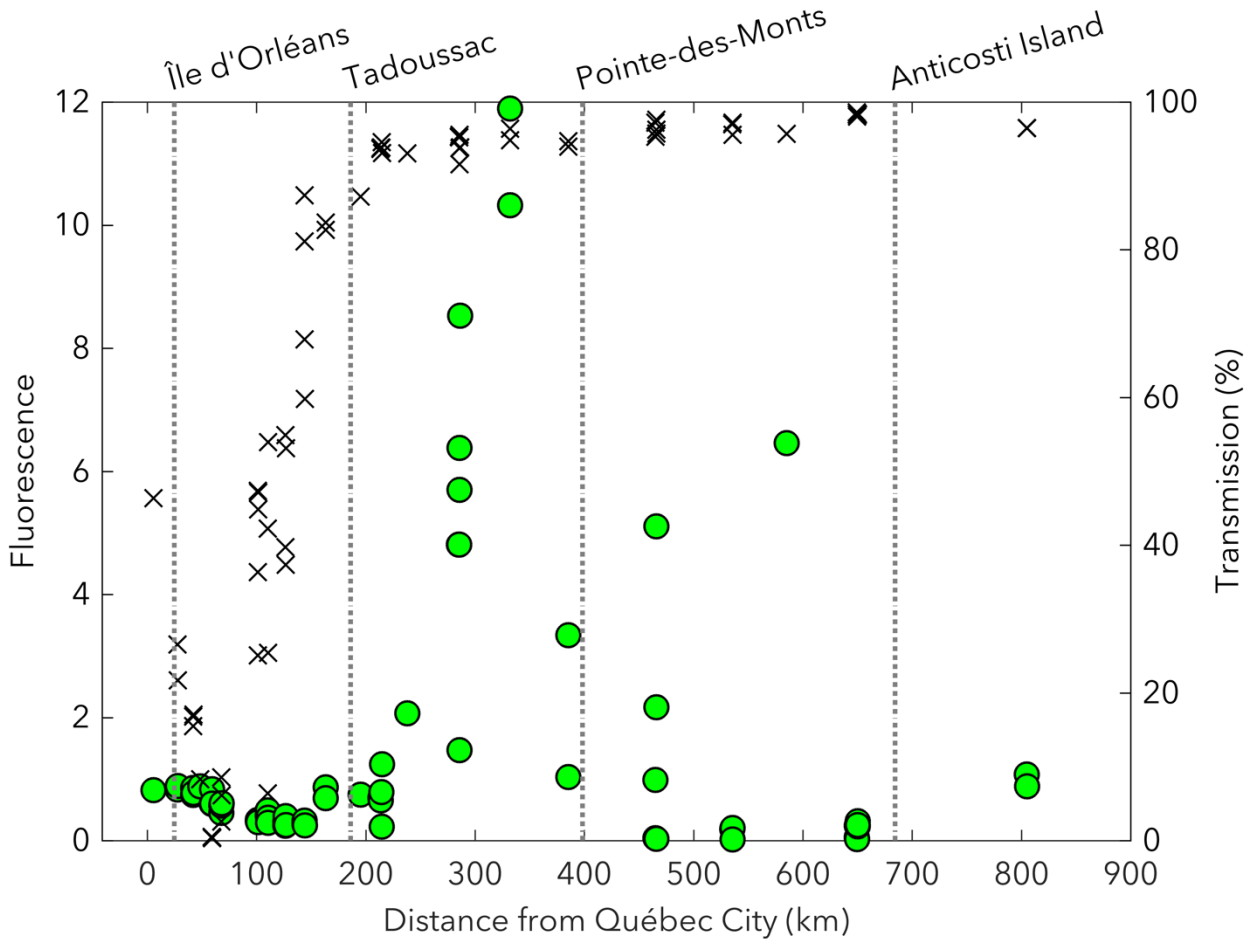

Figure 10. Spatial distributions of maximum fluorescence values (circles) and mean transmission values (x symbols) in the euphotic zone of the St. Lawrence River, Estuary and Gulf during the May 2016 cruise. Fluorescence is a primary production proxy, whereas transmission is an excellent proxy for turbidity (low transmission values are due to light absorption by suspended particulate matter and/or colored dissolved organic matter).